Organization of the apical extracellular matrix during tubular organ formation

J. Luke Woodward[1,3,¶], Jeffrey Matthew[1,¶], Vishakha Vishwakarma[1,4], Ying Xiao[2], and SeYeon Chung[1,*]

1 Department of Biological Sciences, Louisiana State University, Baton Rouge, LA 70803, USA

2 Shared Instrumentation Facility, Louisiana State University, Baton Rouge, LA 70803, USA

3 Present address: Department of Cell and Molecular Biology, University of Chicago, Chicago, IL 60637, USA

4 Present address: Division of Developmental Biology, Eunice Kennedy Shriver National Institute of Child Health and Human Development, National Institute of Health, Bethesda, MD 20892, USA

¶ These authors contributed equally to this study.

*Author for correspondence: seyeonchung@lsu.edu

Keywords: *Drosophila*, salivary gland, apical extracellular matrix, sulfation, Papss, ZP domain proteins, Piopio, Dumpy

Running title: Papss is required for organizing the ZP domain matrix and promoting lumen expansion

Abstract

The apical extracellular matrix (aECM) plays a critical role in epithelial tube morphogenesis during organ formation, but its composition and organization remain poorly understood. Using the *Drosophila* embryonic salivary gland (SG) as a model, we identify Papss, an enzyme that synthesizes the universal sulfate donor PAPS, as a critical regulator of tube lumen expansion. *Papss* mutants show a disorganized apical membrane, condensed aECM, and disruptions in Golgi structures and intracellular trafficking. Additionally, we identify two zona pellucida (ZP) domain proteins, Piopio (Pio) and Dumpy (Dpy), as key components of the SG aECM. In the absence of *Papss*, Pio is gradually lost in the aECM, while the Dpy-positive aECM structure is condensed and dissociates from the apical membrane, leading to a thin lumen. Mutations in *dpy* or *pio*, or in *Notopleural*, which encodes a matriptase that cleaves Pio to form the luminal Pio pool, result in a SG lumen with alternating bulges and constrictions, with the loss of *pio* leading to the loss of Dpy in the lumen. Our findings underscore the essential role of sulfation in organizing the aECM during tubular organ formation and highlight the mechanical support provided by ZP domain proteins in maintaining luminal diameter.

Introduction

Epithelial tubes are critical components of many key biological organs, including the kidney, heart, and lungs. Aberrant tube size leads to common diseases and congenital disorders, such as polycystic kidney disease, asthma, and lung hypoplasia. Tube morphogenesis is regulated by multiple factors, including intracellular mechanisms, intercellular interactions, and interactions between cells and the surrounding extracellular matrix (ECM). Specifically, events at the apical (luminal) surface of a tube play an important role in regulating tube diameter and growth, thereby influencing overall tube shape (Myat & Andrew, 2002). During tubular organ formation, the surrounding epithelium secretes apical ECM (aECM) components into the lumen, where they form the luminal meshwork and interact with the apical membrane, playing a critical role in epithelial morphogenesis and regulation of tube dimensions (Jazwinska et al., 2003; Devine et al., 2005; Luschnig et al., 2006; Wang et al., 2006; Syed et al., 2012; Dong et al., 2014; Drees et al., 2023; Gill et al., 2016; Cohen, Sparacio, et al., 2020).

The aECM has a distinct composition compared to the basal ECM, with a diverse array of components Li Zheng et al., 2020. ZP domain proteins, which are highly conserved across species, are of particular interest and are characterized by a conserved 260 amino acid ZP domain that mediates homo- or heteromeric polymerization into filaments. Initially identified in the extracellular coat of mammalian oocytes, ZP domain proteins have been shown to play a critical role in the organization of specialized apical structures in various tissues in species ranging from worms to humans (Yan et al., 2012; Renner et al., 2007; McAllister et al., 1994; Wong et al., 2000; Cohen, Bermudez, et al., 2020; Plaza et al., 2010; Jovine et al., 2005; Litscher & Wassarman, 2020; Wilkin et al., 2000; Ghosh & Treisman, 2024). Chitin, a biopolymer of N-acetylglucosamine, is another major aECM component that is abundant in invertebrates and some vertebrates (Tang et al., 2015; Liu et al., 2019). In many *Drosophila* and *C. elegans* tissues, chitin forms a network of fibers that provide mechanical support and maintain the integrity of the epithelial layer (Araujo et al., 2005; Devine et al., 2005; Moussian et al., 2006; Tonning et al., 2006; Zhang et al., 2005). Several studies have shown the role of ZP proteins in maintaining the chitin matrix in the aECM. During *Drosophila* tracheal development, two ZP proteins, Dumpy (Dpy) and Piopio (Pio), compose an elastic structure in the lumen that modulates the mechanical stress and maintains the chitin matrix (Jazwinska et al., 2003; Dong et al., 2014; Drees et al.,

2023). In the *Drosophila* corneal lens, another ZP domain protein, Dusky-like, establishes an external scaffold for chitin retention (Ghosh & Treisman, 2024). However, many organs in both vertebrates and invertebrates have the non-chitinous aECM, and the role of ZP proteins in the non-chitinous aECM is less well understood.

Post-translational modifications of the aECM are essential for proper tube dimensions during organ formation (Luschnig et al., 2006; Wang et al., 2006; Abrams et al., 2006; Herman & Horvitz, 1999 Hwang et al., 2003; Cohen, Sparacio, et al., 2020; Cohen & Sundaram, 2020). Sulfation is an abundant post-translational modification that takes place in the Golgi apparatus, where a sulfate group is covalently attached to amino acid residues of proteins or side chains of proteoglycans (Gunal et al., 2019). Studies in a mouse model of cystic fibrosis suggest a link between the disease state and proper sulfation levels in organs Xia et al., 2005, but the role of sulfation in tubular organ development and aECM organization remains elusive. Sulfation reactions require a high-energy form of sulfate, 3'-phosphoadenosine-5'-phosphosulfate (PAPS), which is produced by the enzyme PAPS synthase (Papss) (van den Boom et al., 2012; Gunal et al., 2019). Mammals have two isoforms of Papss, Papss1 and Papss2. *Papss1* shows ubiquitous expression, with higher levels in glandular cells and salivary duct cells, suggesting a high requirement for sulfation in these cell types (Uhlen et al., 2005; Karlsson et al., 2021). *Papss2* shows a more restricted expression in certain tissues such as cartilage, and mutations in *Papss2* have been associated with skeletal dysplasia in humans and mice (Faiyaz ul Haque et al., 1998; Ahmad et al., 1998; Kurima et al., 1998; Ford-Hutchinson et al., 2005). Mouse models with exon deletions in *Papss1* or *Papss2* show more extensive defects, including lethality (*Papss1*) and abnormal craniofacial and limb morphology (*Papss2*) (Groza et al., 2023), suggesting a critical role for Papss in vital developmental processes. *Drosophila* has a single *Papss* gene, allowing for a straightforward investigation of its function in developmental processes without redundancy. By studying the role of *Papss* in *Drosophila* development, we can gain valuable insights into the role of this conserved enzyme in normal development and disease in humans.

To understand the role of post-translational modification in the organization of the aECM and to determine the key composition of the non-chitinous aECM in tubular organs, we use the *Drosophila* embryonic SG as a model. This single-layered epithelial tube is formed through highly stereotyped morphogenetic processes (Chung et al., 2014), making it an excellent system

77 for elucidating the molecular mechanisms underlying aECM composition and modification. SG
78 cells are specified on the ventral surface of the embryo at stage 10. Once specified, SG cells do
79 not undergo cell division or cell death because SG-upregulated transcription factors
80 downregulate the expression of key cell cycle genes and proapoptotic genes (Myat & Andrew,
81 2000a; Chandrasekaran & Beckendorf, 2003; Fox et al., 2013; Matthew et al., 2024), and thus
82 the entire morphogenetic process is driven by cell shape change, cell rearrangement, and
83 collective cell migration (Myat & Andrew, 2000b; Bradley & Andrew, 2001; Bradley et al.,
84 2003; Chung & Andrew, 2014; Chung et al., 2017). At stage 11, SG cells invaginate to form a
85 three-dimensional tubular structure, which then elongates and migrates toward its final position
86 during stages 12-13. The SG continues to migrate and the lumen expands significantly by apical
87 secretion during stages 14-16, forming the fully developed organ. Despite limited knowledge of
88 the composition of the aECM in the SG, previous work has demonstrated the critical role of
89 ADAMTS-A, a secreted metalloprotease, in releasing cells from the aECM to facilitate SG
90 migration and normal lumen shape (Ismat et al., 2013). Our previous work has also shown that
91 cell-aECM adhesion via the apical surface protein Cad99C influences cell rearrangement during
92 SG elongation (Chung & Andrew, 2014).

93 Here, we identified Papss as being essential for aECM organization and lumen expansion
94 of the *Drosophila* embryonic SG. Loss of *Papss* results in a disorganized apical membrane and a
95 condensed aECM, which is associated with disrupted Golgi structures and intracellular
96 trafficking. *Papss* mutants also show defects in the basal ECM and occasional SG cell death,
97 leading to invasion of hemocytes into SG epithelia that engulf dying cells. We identified two ZP
98 proteins, Pio and Dpy, as key components of the SG aECM. In the SG lumen, these ZP domain
99 proteins form a filamentous scaffold that is significantly affected by the loss of *Papss*, with Pio
100 eventually being lost from the aECM and the Dpy-positive aECM structure condensing and
101 dissociating from the apical membrane. Mutations in *pio* or *dpy*, or in *Notopleural* (*Np*), which
102 encodes a matriptase that cleaves Pio to form the luminal pool of Pio, exhibit bulging and
103 constriction of the SG lumen. Notably, mutations in *pio* result in the loss of luminal Dpy signals
104 in the SG. These data indicate that the Dpy-containing filamentous structure of the aECM is
105 crucial for maintaining luminal diameter and that the luminal pool of Pio is essential for
106 organizing this structure during SG morphogenesis.

Results

Papss is required for SG lumen expansion

To identify key enzymes that affect SG morphology by modifying aECM components, we examined the effects of the loss of ~20 enzymes that are highly expressed in the SG and are likely to function in the secretory pathway (Fox et al., 2013). Deficiency lines deleting each enzyme were immunostained with the apical membrane marker Crumbs (Crb) or Stranded at Second (SAS) to assess SG lumen shape and screened for morphological defects. Among the twelve lines showing defects (Table S1), a deficiency line deleting *PAPS synthetase* (*Papss*) and 18 other genes exhibited unique morphological defects: a very thin SG lumen with irregular apical protrusions (Fig. 1A). Papss catalyzes the synthesis of 3'-phosphoadenosine-5'-phosphosulfate (PAPS), the sulfate donor compound in all sulfotransferase reactions (Negishi et al., 2001). Consistent with a previous report (Jullien et al., 1997) and high-throughput RNA in situ hybridization data (Weiszmann et al., 2009), our fluorescence in situ hybridization confirmed that *Papss* transcripts are highly expressed in the SG throughout morphogenesis (Fig. 1B), suggesting a high demand for sulfation in the *Drosophila* SG.

To test the role of *Papss* and confirm the phenotype, we used a *Papss* EMS mutant line (Zhu et al., 2005). The Papss protein contains two critical protein domains, the ATP sulfurylase domain, which adds sulfate to an AMP group of ATP to form adenosine 5’-phosphosulfate (APS), and the APS kinase domain, which phosphorylates APS to form PAPS (Venkatachalam et al., 1998; Yanagisawa et al., 1998). Sanger sequencing of this mutant identified a point mutation (G->A) that introduces a premature stop codon (Trp271->stop) located near the N-terminus of the APS sulfurylase domain, resulting in a truncated protein in which most of the domain is not translated (Sup. Fig. S1A, B). Since both protein domains are essential for the enzyme function of Papss, we conclude that this EMS mutant line is potentially null or a strong hypomorphic allele. *Papss* homozygous mutants and transheterozygotes for *Papss* mutant over a deficiency were embryonic lethal. To test the role of Papss in sulfation in the SG, we performed immunostaining for sulfotyrosine in wild-type (WT) and *Papss* EMS mutant embryos. In WT, we observed strong sulfotyrosine signals both in the apical membrane and as puncta in the cytoplasm of SG cells (Sup. Fig. S2A). The cytoplasmic puncta colocalized with ManII-GFP signals, a medial Golgi marker (Ye et al., 2007), suggesting that proteins undergoing tyrosine

137 sulfation in the Golgi are detected by the antibody (Sup. Fig. S2C). In *Papss* mutants, the
138 cytoplasmic punctate signals were significantly reduced (Sup. Fig. S2B), suggesting that
139 sulfation in the Golgi is decreased. The signals at the apical membrane appeared similar or
140 slightly reduced compared to WT, suggesting that sulfated molecules, possibly by maternally
141 provided Papss, were still targeted apically, although it is not clear whether they were properly
142 targeted to their original destination or mislocalized. Together with a previous study using Alcian
143 Blue staining showing the loss of sulfated biomolecules in the *Papss* mutant SG (Zhu et al.,
144 2005), these data suggest sulfation in the SG is dependent on Papss.

145 *Papss* homozygous mutant embryos often showed defects in overall embryonic
146 morphology, such as defects in germ band retraction and head involution (39%; N=80/204; Sup.
147 Fig. S3A-F). A smaller percentage of transheterozygous embryos showed these defects (10%;
148 N=13/136), with many late-stage embryos appearing normal (Sup. Fig. S3C, E, F). We conclude
149 that transheterozygous embryos with more severe defects did not survive to late stages, but we
150 cannot rule out the possibility that a secondary mutation at another gene locus contributes to the
151 overall embryonic defects. Embryos with these morphological defects often showed defects in
152 SG invagination, forming a SG close to the surface of the embryo (Sup. Fig. S3D, G, H). We
153 used the embryos that formed the SG in the normal position for quantification and further
154 analysis.

155 Using the adherens junction (AJ) marker E-cadherin (Ecad) signals, we analyzed the SG
156 lumen phenotype in *Papss* homozygous mutant embryos and transheterozygotes. During stages
157 14-16, the WT SG lumen expanded consistently throughout its length (Fig. 1C). In contrast,
158 *Papss* mutant embryos exhibited irregularities in SG lumen expansion. At stage 14, when the
159 WT SG lumen expansion began, more than 40% of *Papss* mutant embryos had either a
160 noticeably thinner lumen (Fig. 1D, G; 18%; N=7/38) or a slightly irregular lumen with a small
161 bulge (Fig. 1D, G; 24%; N=9/38). At stage 16, about half of *Papss* mutant embryos showed an
162 overall thin lumen with an irregular apical membrane (Fig. 1D, G'; 51%; N=21/41) and the other
163 half had an irregularly expanded lumen with thin and expanded regions along its length (Fig. 1D,
164 G'; 49%; N=20/41). We quantified SG lumen area at stage 16 in *Papss* mutants with the thin
165 lumen phenotype using Ecad signals and found a significant decrease in lumen area compared to
166 WT (Fig. 1H), suggesting a role for Papss in SG lumen expansion.

167 To determine whether the defects in SG lumen expansion are due to the loss of *Papss*, we
168 performed a rescue experiment by overexpressing Papss in the SG using the SG-specific driver
169 *sage-Gal4* (Chung et al., 2009) in the *Papss* mutant background. *Papss* produces multiple
170 isoforms, including Papss-PA/B/C/G (629 aa), Papss-PD (657 aa), and Papss-PE/F/H (630 aa),
171 which differ only slightly in the N-terminus (Flybase; www.flybase.org). We generated UAS
172 lines for Papss-PD and Papss-PE and found that overexpression of either isoform in the SG of
173 WT embryos resulted in a normally expanded SG lumen (Fig. 1E, G'). Given the high levels of
174 *Papss* mRNA in the WT SG, the Papss protein is likely abundant in the SG, which may explain
175 why further overexpression of Papss does not lead to any additional effects. We chose to use the
176 UAS-Papss-PE line for further experiments (hereafter, Papss-PE will be referred to as Papss
177 when overexpressed). When Papss was overexpressed in the SG of *Papss* mutant embryos, only
178 a very small fraction (4%; N=1/26) showed a thin lumen phenotype along the entire length of the
179 SG (Fig. 1F, G'). The majority of embryos (73%) showed either a normal, fully expanded lumen
180 along the entire length of the SG, with occasional slight irregularities at the apical membrane
181 (42%; N=11/26), or a irregularly expanded lumen, where some parts of the SG lumen were
182 expanded and others were thin (31%; N=8/26) (Fig. 1F, G'). SGs with normally expanded
183 lumens had luminal area comparable to that of WT embryos (Fig. 1H). Interestingly, some of the
184 embryos had an over-expanded SG lumen, often with a non-uniform diameter (24%; N=6/24;
185 Fig. 1F, G'). We speculate that the mutant Papss protein may compete with the overexpressed
186 WT protein, resulting in a variation of rescue effect. Overall, although a range of phenotypes is
187 present, the thin SG lumen phenotype was almost completely rescued by SG-specific expression
188 of Papss.

189

190 **Loss of *Papss* disrupts the apical domain and aECM organization**

191 To investigate the cellular basis of the thin SG lumen phenotype in *Papss* mutants, we examined
192 the localization of key apical membrane proteins and junctional markers. In WT SGs, the apical
193 polarity protein Crb localized to the subapical region between the apical surface (free apical area)
194 and the AJs, and we observed clear Crb signals along the apical cell boundary of each SG cell
195 (Fig. 2A, B). In contrast, *Papss* mutants showed Crb signals dispersed along the entire apical
196 surface of SG cells (Fig. 2C), indicating disorganization of the apical domain. The AJ marker

197 Ecad and the septate junction (SJ) marker Discs large (Dlg) showed no apparent disruption in
198 localization compared to WT (Sup. Fig. S4A-E). These data suggest that loss of *Papss* disrupts
199 the apical membrane in the SG, while leaving the junctional regions intact.

200 Next, we investigated the organization of the aECM, using wheat germ agglutinin (WGA),
201 which marks several glycan modifications including O-linked β-N-acetylglucosamine (O-
202 GlcNAc). WGA labels the apical membrane and luminal structure in the *Drosophila* embryonic
203 trachea (Tonning et al., 2005; Chung et al., 2009). Similarly, we observed WGA signals in the
204 apical membrane and the lumen of WT SGs (Fig. 2D). Both pools of WGA signals were relatively
205 weak. Notably, the luminal signals showed multiple thin filamentous organizations traversing the
206 lumen (Fig. 2D), suggesting a heterogeneity of the luminal structure. In *Papss* mutants, WGA
207 signals were increased in both the lumen and apical membrane, with the apical membrane signals
208 appearing more diffuse (Fig. 2E). Interestingly, the luminal WGA signals in *Papss* mutants
209 accumulated strongly on one side along the entire length of the lumen, whereas the thin filamentous
210 WGA signals in WT SGs appeared to show no bias and were mostly centered in the lumen. In
211 regions with a thin SG lumen, WGA was present in a highly condensed rod-like structure; in
212 expanded regions, WGA signals showed either a similar condensed rod-like structure favoring one
213 side of the SG lumen or a slightly condensed filamentous structure often broadly associated with
214 the apical membrane (Fig. 2E). Transmission electron microscopy (TEM) analysis also revealed
215 highly condensed and more electron-dense luminal structures in the SG of *Papss* mutants
216 compared to WT (Fig. 2G, H). SG-specific overexpression of Papss in the *Papss* mutant
217 background resulted in less condensed luminal WGA structures compared to *Papss* mutants, which
218 were mostly localized in the center of the SG lumen. These aECM structures were not as thin as
219 in WT (Fig. 2F), suggesting a partial rescue of the aECM structure. The partial rescue of the
220 luminal structure is consistent with a variation in lumen expansion phenotypes observed in the
221 rescue experiment (Fig. 1F, G'). Taken together, these data suggest a role for Papss in the proper
222 organization of the SG aECM witht loss of *Papss* resulting in a tightly packed or condensed aECM
223 that is loosely associated with the apical membrane.

224

225 **Loss of *Papss* disrupts Golgi organization and mislocalizes intracellular trafficking**
226 **markers**

227 In addition to apical membrane and luminal signals, we detected WGA signals in several large
228 cytoplasmic punctate structures in WT SG cells, mirroring the sulfotyrosine signals in the Golgi
229 (Fig. 3A; Sup. Fig. S2B). These punctate WGA signals colocalized with the medial-Golgi marker
230 ManII-GFP and, like sulfotyrosine signals, were significantly reduced in *Papss* mutants (Fig. 3A,
231 B). When Papss was specifically overexpressed in the SG, the WGA signals in cytoplasmic puncta
232 were partially restored (Fig. 3C), suggesting that the defective Golgi structures are likely rescued.
233 We also observed WGA signals around the nucleus (Fig. 3A), consistent with a role for WGA in
234 binding to glycoproteins on the nuclear envelope (Rutherford et al., 1997). The intensity of these
235 signals was also significantly reduced in *Papss* mutants (Fig. 3B). Interestingly, we observed
236 highly dispersed ManII-GFP signals in *Papss* mutants SGs (Fig. 3D, E), suggesting that Golgi
237 structures may be disrupted. To examine the Golgi structures in more detail, we performed TEM
238 analysis in WT and *Papss* mutant SG cells. In contrast to the mammalian Golgi, the *Drosophila*
239 Golgi lacks the characteristic ribbon-like structure and is composed of a series of individual
240 cisternae arranged in a random, disordered fashion (Kondylis & Rabouille, 2009). While the Golgi
241 in WT SG cells showed randomly arranged cisternae, the Golgi in *Papss* mutants showed abnormal
242 arrangement, either stacked or compressed, with small electron-dense puncta along these structures
243 (Fig. 3F, G), suggesting a functional defect and possible protein aggregation. These data suggest
244 that loss of *Papss* disrupts Golgi structures, which could lead to trafficking defects and
245 abnormalities in the post-translational modification of proteins traversing the secretory pathway.

246 Other organelles, such as the endoplasmic reticulum (ER), appeared relatively normal. SG-
247 specific expression of GFP-KDEL, GFP fused to the ER retention motif KDEL, or immunostaining
248 for prolyl-4-hydroxylase-alpha SG1, an ER-resident enzyme (Abrams et al., 2006), showed no
249 significant differences between WT and *Papss* mutant SGs (Sup. Fig. 5A-D). TEM analysis also
250 revealed similar ER structures in WT and *Papss* mutant SG cells (Sup. Fig. 5E, F). These data
251 suggest that loss of *Papss* does not disrupt the ER.

252 The aberrant Golgi structures observed in *Papss* mutants prompted us to investigate the
253 impact on intracellular trafficking components. We examined the localization of Rab11, a marker
254 for recycling endosomes, Rab7, a marker for late endosomes, and Sec15, an exocyst marker. As
255 previously shown (Chung & Andrew, 2014; Le & Chung, 2021, Rab11 and Sec15 were enriched
256 along the apical domain of WT SG cells (Fig. 3H, J). In *Papss* mutants SGs, we observed an

257 increase in apical Rab11 signal intensity, with some signals mislocalized to the basolateral region
258 (Fig. 3I, L). In contrast, Sec15 signals were significantly reduced at the apical membrane (Fig. 3K,
259 M). Unlike Rab11 or Sec15, Rab7 localized in large punctate structures in the cytoplasm in WT
260 SG cells (Sup. Fig. S6A). In *Papss* mutants, the number of Rab7 puncta was significantly reduced,
261 although the intensity of Rab7 puncta was not significantly different from WT (Sup. Fig. S6B-D).
262 TEM analysis revealed a number of electron-dense vesicles in the apical domain of SG cells in
263 WT (Fig. 3N). In contrast, *Papss* mutant SGs showed fewer electron-dense vesicles, but instead
264 we observed several larger, empty vesicle-like structures (Fig. 3O, P). Collectively, these data
265 suggest that defective sulfation affects Golgi structures and multiple routes of intracellular
266 trafficking, with apical trafficking being significantly impaired.

267

268 **Loss of *Papss* results in abnormal cell death and disruption of the basal ECM**

269 In *Papss* mutant embryos, we often observed one or more acellular regions within the SG
270 epithelium during late embryogenesis that lacked any markers for nuclei, cell membranes, or
271 junctions. To test whether these acellular regions were caused by cell death, we stained embryos
272 with an antibody against *Drosophila* cleaved death caspase-1 (DCP-1; Sarkissian et al., 2014).
273 Indeed, DCP-1 signals were often found within the acellular spaces (Fig 4A, B), suggesting that
274 loss of *Papss* leads to abnormal cell death in the SG. TEM analysis also captured a dying cell in
275 the *Papss* mutant SG providing further evidence to support the occurrence of apoptotic cell death
276 (Fig. 4C). Quantification of the number of SG cells at stage 16 revealed that *Papss* homozygous
277 embryos and transheterozygous embryos over a deficiency have significantly fewer cells than
278 WT (Fig. 4D). SG-specific overexpression of Papss in the *Papss* mutant background rescued the
279 decreased SG cell number phenotype (Fig.4D), suggesting that Papss is required for SG cell
280 survival. Blocking apoptosis in the *Papss* mutant SG by overexpressing the baculoviral protein
281 p35, a caspase inhibitor of apoptosis, also restored the SG cell number (Fig. 4D). This suggests
282 that apoptosis is a key mechanism underlying SG cell loss in *Papss* mutants. Importantly, the
283 SGs in these embryos still showed the thin (25%; N=2/8) or irregularly expanded (75%; N=6/8)
284 lumen phenotypes, suggesting that the defects in SG lumen expansion in *Papss* mutants are
285 independent of abnormal cell death.

286 Using srpHemo3x-mCh (Gyoergy et al., 2018), we labeled hemocytes, which are
287 analogous in function to macrophages in vertebrates. Hemocyte signals were often present in the
288 acellular regions of the SG in *Papss* mutants, suggesting that hemocytes may aid in apoptotic cell
289 clearance from the SG epithelium (Fig. 4E, F). In normal epithelia, the basal ECM acts as a
290 physical barrier, preventing hemocytes from migrating into the epithelial layer. To examine the
291 integrity of the basal ECM in *Papss* we used an antibody against Nidogen (Ndg), a glycoprotein
292 with important linker functions in the basement membrane (Aumailley et al., 1993). Ndg-
293 positive basal ECM was detected in a regular, thin layer around WT SGs at stage 16 (Fig. 4G).
294 However, in *Papss* mutants, Ndg signals were irregular and often disconnected, and we observed
295 hemocytes invading SG cells through the gaps in the Ndg-positive basal ECM (Fig. 4H). Overall,
296 our data suggest that loss of *Papss* leads to aberrant cell death in the SG and disrupts both the
297 apical and basal ECM of the SG.

298

299 **The ZP domain proteins Pio and Dpy of the SG aECM are affected by the loss of *Papss***

300 To better understand how aECM composistion and organization are affected by *Papss* loss, we set
301 out to identify components of the SG aECM. Since chitin, a major aECM component in many
302 *Drosophila* tissues, is absent from the SG lumen (Fig. 5A), we focused on ZP domain proteins. Of
303 the 18 ZP domain proteins in *Drosophila*, at least six are expressed in the embryonic SG, including
304 *pio*, *dp*y, *quasimodo* (*qsm*), *cypher* (*cyr*), *dusky* (*dy*), and *CG17111* (Tomancak et al., 2002;
305 Jazwinska & Affolter, 2004; Weiszmann et al., 2009). We tested Pio and Dpy, key aECM
306 components critical for *Drosophila* tracheal morphogenesis (Jazwinska et al., 2003; Drees et al.,
307 2023), and Qsm, which plays a critical role in remodeling Dpy in the aECM during *Drosophila*
308 flight muscle development (Chu & Hayashi, 2021).

309 To test Pio localization in the SG, we used a transgenic line expressing an mCherry-Pio
310 (mCh-Pio) fusion protein with the N-terminal mCh tag (Drees et al., 2023; Fig. 5B), as well as a
311 Pio antibody generated with the peptide corresponding to the sequence within the ZP domain of
312 Pio, between the ZP-N and ZP-C domains (Jazwinska et al., 2003; Fig. 5B). mCh-Pio signals were
313 observed in cytoplasmic puncta, at the apical membrane, and in the SG lumen. These signals,
314 especially the luminal signals, became stronger at stages 15-16 (Fig. 5C), suggesting that Pio is

315 transported apically and secreted into the SG lumen. Pio antibody signals (hereafter Pio signals)
316 showed a similar, but still distinct, localization, predominantly in the SG lumen and at the apical
317 membrane. At stages 11 and 12, low levels of cytoplasmic punctate signals were detected along
318 with strong luminal signals, but from stage 13, Pio signals were predominantly localized to the SG
319 lumen (Fig. 5D, E; Fig. S7A). Interestingly, compared to the diffuse luminal mCh-Pio signals (Fig.
320 5C), Pio signals in the SG lumen showed heterogeneity with filamentous structures (Fig. 5E-F''),
321 similar to the luminal WGA signals. Pio signals were absent at all stages in the *pio* null mutant, in
322 which the entire ZP domain is deleted (Drees et al., 2023; Fig. S7B, C), confirming the specificity
323 of the antibody. The Pio protein is known to be cleaved, at one cleavage site after the ZP domain
324 by the furin protease and at another cleavage site within the ZP domain by the matriptase
325 Notopleural (Np) (Drees et al., 2019; Drees et al., 2023; Fig. 5B). The latter cleavage site falls
326 within the peptide sequence used to generate the Pio antibody (Fig. 5B). A possible explanation
327 for the different signals between mCh-Pio and Pio signals is that the Pio antibody preferentially
328 recognizes the C-terminal ZP domain fragment after furin and Np cleavage, whereas diffuse,
329 luminal mCh-Pio signals are either the secreted Pio protein cleaved only by furin or the N-terminal
330 fragment after Np cleavage.

331 Dpy-YFP signals from the Dpy-YFP transgenic line (Lye et al., 2014) showed
332 heterogeneous, filamentous structures in the SG lumen throughout SG morphogenesis (Sup. Fig.
333 S8A) that colocalized with Pio and WGA signals (Fig. 8E-F"; Sup. Fig. S8C). It should be noted
334 that because homozygous Dpy-YFP embryos showed a bulging and constricted SG lumen
335 phenotype with highly condensed Dpy-YFP signals throughout the lumen (Sup. Fig. S8B), we
336 used embryos with one copy of the transgene to analyze Dpy localization. Unlike Pio and Dpy,
337 Qsm signals from the Qsm-mCh line (Chu & Hayashi, 2021) were not detected in the SG lumen,
338 suggesting that Qsm is not a component of the SG aECM. Instead, Qsm-mCh signals showed a
339 dynamic intracellular localization during SG morphogenesis. At stages 11-14, Qsm-mCh localized
340 throughout the cytoplasm of SG cells, with increased localization at the apical membrane (Sup.
341 Fig. S9A). At late stage 14/early stage 15, the uniform cytoplasmic signals of Qsm-mCh began to
342 decrease, and Qsm-mCh-positive vesicles formed near the apical domain and coalesced around
343 SJs and the apical membrane. A few Qsm-mCh-positive vesicles were also observed in the basal
344 region of SG cells. At stage 16, Qsm-mCh signals decreased in vesicles and instead increased at

345 the apical membrane and were clearly detected at SJs, colocalizing with Dlg (Fig. S9B). Taken
346 together, our data suggest that Pio and Dpy form filamentous aECM structures in the SG.

347 We next examined Pio, mCh-Pio, Dpy-YFP, and Qsm-mCh signals in *Papss* mutant SGs
348 at stages 14 and 16. At stage 14, Pio and Dpy-YFP signals appeared condensed and enriched
349 within the SG lumen, with reduced association with the apical membrane compared to WT (Fig.
350 5G, G'). Interestingly, Pio signals were barely detectable in the SG lumen at stage 16 (Fig. 5H-
351 H'''), likely due to either protein degradation or epitope masking caused by aECM condensation
352 and protein misfolding. In contrast, Dpy-YFP signals remained in the lumen at all stages and
353 were condensed and localized to one side of the lumen at stage 16 (Fig. 5H-H'''), similar to
354 WGA signals (Fig. 2E). mCh-Pio signals in *Papss* mutants were comparable to the control (Fig.
355 5D). We also did not observe any significant differences in the localization or intensity of Qsm
356 signals in *Papss* mutants, although Qsm signals occasionally appeared slightly diffuse at SJs in
357 *Papss* mutants (Sup. Fig. S9C). These data suggest that the luminal pool of Pio and Dpy, which
358 form filamentous structure, is significantly affected by the loss of *Papss*, resulting in the loss of
359 Pio and the condensation and dissociation of the Dpy-containing aECM structure from the apical
360 membrane.

361

362 **ZP domain matrix is required for uniform SG lumen diameter**

363 We next investigated the role of Pio and Dpy in SG morphogenesis by analyzing SG lumen
364 morphology in *pio* and *dpy* mutants. Immunostaining with Ecad revealed that *pio* null mutants
365 formed relatively normal SGs up to stage 15, but stage 16 SGs showed dramatically abnormal
366 luminal morphology characterized by bulging and constriction, often with multiple constrictions
367 (Fig. 6A, B; Sup. Fig. S10A-B). The constricted regions were severely narrowed to the point of
368 almost no luminal space, and the bulging regions occasionally showed a flat protrusion on one side
369 of the SG lumen (Fig. 6C). Notably, these abnormal luminal shapes were associated with a
370 progressive loss of luminal WGA and Dpy-YFP signals (Fig. 6D). In *pio* mutants, WGA signals
371 were comparable to WT at stages 13 and 14 (Sup. Fig. S10A-B), but appeared slightly reduced
372 and diffuse in the SG lumen at stage 14, and this reduction became more pronounced at stage 15
373 (Fig. 6A, B). Dpy-YFP signals were more severely affected in *pio* mutants. Unlike the strong,

374 filamentous luminal signals in the control (Sup. Fig. S8A), Dpy-YFP signals were reduced and
375 diffuse in the SG lumen and were detected in the cytoplasm of *pio* mutant SG cells from stage 12
376 to stage 14, with a conspicuous absence in the lumen at stage 15 (Sup. Fig. S10C). By stage 16,
377 both WGA and Dpy-YFP signals were completely absent from the lumen in *pio* mutants, whereas
378 the signals were still present at the apical membrane and in the cytoplasm (Fig. 6B, D).

379 To test a role for Pio cleavage and localization in shaping the SG lumen, we analyzed embryos
380 mutant for the matriptase Np, which cleaves Pio. In *Np* mutants, Pio and WGA signals were
381 observed in both the apical membrane and lumen up to stage 14, similar to WT embryos (Fig. 6E).
382 However, at stage 16, Pio signals were observed closely associated with the apical membrane, with
383 no filamentous luminal Pio signals present (Fig. 6E), suggesting that Np is required for this luminal
384 pool of Pio. Importantly, *Np* mutants exhibited the same bulging and constricting SG luminal
385 phenotype at stage 16 as *pio* mutants (Fig. 6E), indicating that the filamentous luminal Pio structure
386 plays a crucial role in maintaining a uniform SG diameter.

387 *dpy* mutants (dpy^{ov1}) exhibited a more severe bulging and constriction phenotype in the SG lumen
388 compared to *pio* mutants. Until stage 14, SGs in *dpy* mutants often showed a curved shape, but
389 otherwise had a relatively normal morphology and uniform diameter (Sup. Fig. S10C). At stages
390 15 and 16, SG lumen lost regularity and uniformity, often exhibiting multiple bulges and
391 constrictions. (Fig. 6F). In constricting regions, we observed condensed Pio and WGA signals in
392 the lumen, whereas in bulging regions, weak Pio and WGA signals were detected along the apical
393 boundaries (Fig. 6F). These data suggest a disrupted luminal scaffold that correlates with the
394 bulging and constricting luminal morphology. Taken together, our data suggest that Dpy and Pio
395 form a luminal scaffold necessary for a uniform SG tube diameter and that Pio cleavage by Np is
396 essential for maintaining this scaffold.

397

398 **Discussion**

399 Our study highlights the critical role of Papss, a key enzyme that produces the universal sulfate
400 donor PAPS, in aECM organization and lumen expansion in the *Drosophila* embryonic SG.
401 *Papss* mutants show defective SG lumen expansion, accompanied by disruption of the apical
402 domain of SG cells and the aECM. The loss of *Papss* leads to defective intracellular trafficking,
403 abnormal cell death in the SG, and defective basal ECM, emphasizing the importance of
404 sulfation in multiple developmental processes. We also identify the ZP domain proteins Dpy and
405 Pio as key components of the SG aECM, where Dpy is a scaffolding aECM structure that
406 provides mechanical support and Pio is required for proper organization of this structure.

407

408 **Sulfation is critical for aECM organization and SG lumen expansion**

409 During *Drosophila* SG morphogenesis, secreted cargos are modified in the Golgi, secreted
410 apically, and deposited in the lumen to form the aECM meshwork. Our data show that sulfation
411 is essential for the proper organization of the aECM and the formation of a normal SG luminal
412 shape. Consistent with a high demand for sulfation in the SG, transcripts for *Papss* and several
413 other key enzymes involved in sulfation reactions are also upregulated in the SG, including
414 *slalom* (*sll*), which encodes the *Drosophila* PAPS transporter (Kamiyama et al., 2003; Luders et
415 al., 2003), and *pipe* (*pip*) and *tyrosylprotein sulfotransferase* (*Tpst*), which encode
416 sulfotransferases (Suiko et al., 1992; Zhu et al., 2005). Notably, Alcian Blue-stained materials
417 are absent from the SG in *Papss*, *sll*, or *pip* mutants Zhu et al., 2005, suggesting that sulfation in
418 the SG depends entirely on these enzymes. Our data show that the irregularly expanded SG
419 lumen phenotype in *Papss* mutants is associated with the condensed aECM structures and
420 reduced association of the aECM with the apical membrane (Figs. 1 and 2). Inappropriate charge
421 balance due to defective sulfation of proteoglycans and glycoproteins, as well as protein
422 misfolding or failure to bind to appropriate partners, may contribute to aggregation of aECM
423 components and condensation of the aECM structure. The ubiquitously expressed human *Papss1*
424 gene shows upregulation in several glandular organs and the salivary duct (Uhlen et al., 2005;
425 Karlsson et al., 2021), suggesting a potentially conserved role for this enzyme in modifying
426 secreted molecules and modifying aECM in these organs.

427 The defects in SG lumen expansion in *Papss* mutants are linked to defects in intracellular
428 trafficking, characterized by aberrant Golgi structures and mislocalized or reduced levels of
429 several vesicle markers (Fig. 3). This suggests that the loss of *Papss* has a broader impact on the
430 intracellular trafficking system, beyond the sulfation of specific substrate molecules. Consistent
431 with the idea that the secretory pathway plays a key role in trafficking aECM components to the
432 lumen, several mutants in intracellular trafficking genes, such as *CrebA*, *Sec61β*, and *Sar1*,
433 which encode a major transcription factor that boosts secretory capacity, a Sec61 translocon
434 component, and a COPII vesicle formation component, respectively, have been shown to have a
435 slightly thinner SG lumen (Fox et al., 2013; Fox & Andrew, 2015). However, the defects in
436 *Papss* mutants differ from those in general secretion mutants. While the latter exhibit a
437 uniformly thin lumen, altered localization of several subcellular organelles including
438 mitochondria and the ER, and reduced Golgi signals (Fox & Andrew, 2015), *Papss* mutants
439 show an irregularly expanded lumen and primarily affect the Golgi, while other organelles
440 remain largely intact (Fig. 3; Fig. S5). Some of the abnormally modified targets appear to be
441 aggregated in the defective Golgi, but many are still transported apically and secreted into the
442 lumen, resulting in a highly condensed luminal aggregate.

443

444 **The role of ZP domain proteins in non-chitinous aECM in the SG**

445 We are beginning to understand the structural components and biological functions of the non-
446 chitinous aECM during tubular organ formation. For example, in the non-chitinous aECM of the
447 *C. elegans* vulva and excretory duct, distinct aECM components, including zona pellucida (ZP)
448 domain proteins, chondroitin proteoglycans, and glycoproteins, work together to form the lumens
449 of these tubular organs (Gill et al., 2016; Cohen, Sparacio, et al., 2020). Our work reveals that
450 two ZP proteins, Dpy and Pio, play essential roles in organizing the aECM in the *Drosophila* SG,
451 highlighting the important role of ZP proteins in forming the non-chitinous luminal matrix
452 during tubular organ formation. Dpy, a gigantic protein (>2 MDa) with hundreds of epidermal
453 growth factor (EGF) repeats interspersed with a Dpy module, forms long filamentous structures
454 (Wilkin et al., 2000). With these filamentous structures, Dpy plays an essential role in the
455 organization and attachment of apical structures in several tissues, including the thoracic cuticle
456 (Wilkin et al., 2000), embryonic trachea (Jazwinska et al., 2003), pupal wings (Bokel et al.,

457 2005), genitalia (Smith et al., 2020), and muscle tendon cells (Chu & Hayashi, 2021). In the SG,
458 aberrantly formed or lost luminal Dpy structures correlate with abnormal luminal morphology
459 (Figs. 5 and 6; Fig. S8). We propose that the Dpy filamentous structure provides mechanical
460 support in the SG aECM and that proper organization of these structures is critical for the
461 formation of a uniform tube diameter. Our data also suggest that Dpy forms the filamentous
462 luminal structure with Pio. Pio is required to secrete and maintain Dpy in the lumen of the SG
463 (Fig. 6). This is consistent with a role for Pio in Dpy secretion in the *Drosophila* trachea (Drees
464 et al., 2023) and suggests a conserved role for Pio in multiple tissues. Since the ZP domains of
465 Pio and Dpy have been shown to bind directly to each other in vitro (Drees et al., 2023), it is
466 likely that the binding of Pio and Dpy is required for the formation of filamentous luminal
467 structures. This binding may require cleavage of Pio by the matriptase Np, which generates the
468 filamentous luminal pool of Pio (C-terminal ZP fragment of Pio). *pio* and *Np* mutants show
469 similar bulging and constricting SG lumen morphology (Fig. 6), suggesting that the generation of
470 the C-terminal ZP fragment of Pio by Np is critical for the formation of the filamentous luminal
471 structure with Dpy.

472 Papss is required to maintain Pio in the lumen (Fig. 5), suggesting an essential role for
473 sulfation in the formation of the filamentous Dpy/Pio structure (Fig. 5). The ZP domain can
474 mediate homomeric or heteromeric polymerization into filaments, and its structure is stabilized
475 by disulfide bonds formed between conserved Cys residues responsible for the polymerization of
476 ZP modules (Jovine et al., 2002). Defective sulfation in *Papss* mutants may lead to
477 destabilization of Pio-Dpy interactions. Additionally, hundreds of epidermal growth factor (EGF)
478 modules in the Dpy protein are highly susceptible to O-glycosylation. Sulfation of the glycan
479 groups attached to Dpy may be critical for its ability to form a filamentous structure. In the
480 absence of sulfation, the glycan groups on Dpy may not properly interact with the surrounding
481 materials in the lumen, resulting in an aggregated and condensed structure.

482 It will be interesting to determine the role of other ZP proteins highly expressed in the SG.
483 Qsm, for example, has been found in the same intracellular vesicles as Dpy in *Drosophila* tendon
484 cells and has been shown to physically interact with Dpy through their ZP domains (Chu &
485 Hayashi, 2021). Qsm has been shown to remodel Dpy filaments that link tendon cells to the pupal
486 cuticle, increasing their tensile strength (Chu & Hayashi, 2021). In the SG, we find that Qsm is

487 mainly localized to cytoplasmic vesicles and AJ/SJ regions rather than being present in the SG
488 lumen like Pio and Dpy. Further investigation will be needed to determine the role of Qsm in
489 junctional regions of SG cells. Also, the roles of other SG-upregulated ZP domain proteins, such
490 as Dy, Cyr, and CG17111, remain to be elucidated.

491 In conclusion, our analysis of the *Drosophila Papss* gene, a single ortholog of human
492 Papss1 and Papss2, reveals its multiple roles during SG development. We expect that these
493 findings will provide important insights into the function of these enzymes in normal
494 development and disease in humans. Our findings on the key role of two ZP proteins, Pio and
495 Dpy, as major components of the SG aECM also provide valuable information on the
496 organization of the non-chitinous aECM during organ formation.

497

498 **Materials and Methods**

499 **Fly stocks and genetics**

500 The fly stocks used in this study are listed in Table S2. All the crosses were performed at 25°C.

501

502 **Generation of *UAS-Papss* transgenic lines**

503 UAS lines for the Papss-PD (657 aa) and Papss-PE/F/H (630 aa; hereafter referred to as Papss-
504 PE) isoforms were generated. Papss-PD and Papss-PE differ only slightly in the N-terminus.
505 Two UAS clones, UFO09742 (DGRC Stock 1643418;
506 https://dgrc.bio.indiana.edu//stock/1643418 ; RRID:DGRC_1643418) and UFO09743 (DGRC
507 Stock 1643419 ; https://dgrc.bio.indiana.edu//stock/1643419 ; RRID:DGRC_1643419), were
508 obtained from the *Drosophila* Genomics Resource Center. UFO09742 was generated from the
509 RE15281 cDNA clone encoding the open reading frame (ORF) for the Papss-PD isoform.
510 UFO09743 was generated using the RE03925 cDNA clone, which encodes the same OFR for the
511 Papss-PE isoform. Each clone contains a C-terminal Flag-HA tag. Purified DNA for the UAS
512 clones (500 ng/µl) was sent to GenetiVision (Houston, TX) for injection. GenetiVision
513 performed PhiC31-mediated insertions using the attP40 site.

514

515 **Immunostaining and confocal microscopy**

516 *Drosophila* embryos were collected on a grape juice agar plate. All embryos were dechorionated
517 by incubation in 50% bleach for three minutes at room temperature. After dechorionation,
518 embryos were fixed in either standard formaldehyde fixative (7 ml heptane, 5.6 ml ddH_2O, 700
519 µl 37% formaldehyde, 700 µl 10x PBS) or saturated heptane. Saturated heptane was prepared by
520 mixing heptane:37% formaldehyde 1:1 and shaking vigorously. For staining using the
521 horseradish peroxidase (HRP) reaction for visualization, embryos were fixed in formaldehyde
522 fixative and devitellinized by vortexing in 100% methanol. For immunofluorescence staining,
523 embryos were fixed in saturated heptane for forty minutes at room temperature, devitellinized by
524 vortexing in 80% ethanol, and then washed three times in absolute ethanol. Fixed embryos were

525 stained with primary and secondary antibodies in PBSTB (1X PBS, 0.2% bovine serum albumin,
526 and 0.1% Triton X-100). All antibodies used are listed in Table S3. Embryos were then mounted
527 in Aqua-Poly/Mount (Polysciences, Inc). Confocal images were taken using a Leica TCS SP8
528 confocal microscope with 63x, NA 1.4 and 40x, NA 1.3 objectives. HRP images were taken
529 using a Leica DM2500 microscope using a 20x, 0.8 NA objective.

530

531 **Fluorescence in-situ hybridization**

532 In situ hybridization in WT embryos was performed as described in Knirr et al., 1999. Embryos were
533 fixed in a standard formaldehyde fixation, followed by devitellinzation by 100% methanol. To make the
534 *Papss* mRNA probe, a portion of the Papss ORF was amplified using the *UAS-Papss-PD* construct as a
535 template and the primers listed below. Digoxigenin (DIG)-labeled RNA probe was generated by
536 transcribing amplified and purified DNA using SP6 RNA polymerase and DIG RNA labeling mix
537 (Sigma).

538 Forward Primer *Papss*: 5'-ACAAGGATGCGGGTCTGAAG-3'
539 Reverse Primer *Papss* (SP6 RNA polymerase promoter sequence underlined): 5'-
540 G<u>ATTTGGTGACACTATAG</u>CGCCTTAACTCGTTGGGAG-3'

541 Following hybridization, the RNA probe was detected using a sheep α-DIG antibody (Enzo;
542 ENZ-ABS302-0001; 1:1,000). The secondary antibody, α-sheep IgG conjugated with biotin
543 (Invitrogen; 1:500), was visualized using a tyramide reaction with Cy3 (Perkin Elmer Life
544 Sciences, NEL753001kt; 1:50). The embryos were mounted in Aqua-Poly/Mount. Confocal
545 images were taken using a Leica TCS SP8 confocal microscope with 63x, NA 1.4 and 40x, NA
546 1.3 objectives.
547

548 **Genomic DNA sequencing of the Papss open reading frame region in *Papss*^{2} mutant**

549 *Papss*^{2} homozygous mutant embryos were sorted for GFP signals in the balancer chromosome, and
550 genomic DNA was extracted from them. The open reading frame of *Papss* was amplified using the
551 isolated genomic DNA as a template, with the following primers.

552 Primer forward *Papss*: 5'-CTACAGGTGGCGACGAATGT-3'

553 Primer reverse *Papss*: 5'-GCGGCAGGTTCTGGTAGTAG-3'

554 Sanger sequencing of the amplified DNA segment of *Papss* was performed using the primers
555 below.

556 Forward primer 1: 5'-ACAGGTGGCGACGAATGTG-3'
557 Forward primer 2: 5'-TGACCGAGCAAAAGCACCAT-3'
558 Forward primer 3: 5'-CGAGGTGGCCAAGTTGTTTG-3'
559 Forward primer 4: 5'-CCCGAGTTCTACTTTCAGCGT-3'
560 Forward primer 5: 5'-GCCGGTGCGAACTTCTACAT-3'
561 Reverse primer: 5'-GCGGCAGGTTCTGGTAGTAG-3'
562

563 **Quantification of SG cell number**

564 Confocal images immunolabeled with CrebA for stage 16 SGs were used. 3D images for SGs were
565 generated using Imaris (Andor), and SG nuclei were counted using cell ID numbers. Data were
566 displayed using GraphPad Prism, and statistical significance was determined by one-way ANOVA.

567

568 **Quantification of SG lumen area**

569 Confocal images immunolabeled with Ecad for stage 16 SGs were used. Z-stacks were merged to
570 encompass the entirety of the SG lumen. Using Fiji (NIH), images were set to scale according to image
571 properties listed in LasX files. The polygon selection tool was used to outline the entirety of the SG
572 lumen, excluding the SG duct. SG lumen areas were determined for WT, *Papss* thin, and *Papss*
573 irregularly expanded respectively. Statistical significance was determined using a nonparametric t-test as
574 the data did not fit a Gaussian distribution.

575

576 **Quantification for Rab11 and Sec15 apical region intensity**

577 Single z-sections halfway through the proximal-distal axis from confocal images for stage 16 SGs
578 immunolabeled for Rab11 or Sec15 and Ecad were used for quantification. Threshold images for Sec15
579 or Rab11, which display pixels as black or white based on whether they are above a value for signal
580 intensity, were generated in Adobe Photoshop. In addition, Sec15 and Rab11 images were converted
581 using the RGB stack function in Fiji. A stack of images including the threshold and RGB stack
582 converted images for Sec15 or Rab11 and the Ecad images was generated using the images to stack
583 function in Fiji. Using the threshold images for Sec15 and Rab11, a boundary for the apical region
584 encompassing five SG cells, and the mean gray value intensity was calculated from the RGB stack
585 converted Rab11or Sec15 images. The graph was generated in GraphPad Prism, and statistical
586 significance was calculated using Welch's t-test.

587

588 **Quantification for Rab7 puncta number and intensity**

589 Single z-sections halfway through the proximal-distal axis from confocal images for stage 16 SGs
590 immunolabeled for Rab7 and Ecad were used for quantification. Threshold images for Rab7, which
591 display pixels as black or white based on whether they are above a value for signal intensity, were
592 generated in photoshop. Rab7 images were converted using the RGB stack function in Fiji. A stack of
593 images including the threshold and RGB stack converted images for Rab7 and Ecad images were
594 generated using the images to stack function in Fiji. Using the threshold images for Rab7, a boundary
595 was drawn around all puncta present in five cells for each sample, and the mean gray value intensity and
596 area was calculated for the RGB stack Rab7 converted image. The average mean gray value of punctate
597 intensity and the average number of punta in each cell were calculated using Fiji. Punta with an area
598 greater than or equal to 0.100 μm^2 were used for quantification. Statistical significance was calculated
599 by Welch's t-test using GraphPad Prism.

600

601 **Transmission electron microscopy (TEM)**

602 Stage 15 embryos were fixed in 2% glutaraldehyde in 0.2 M phosphate buffer pH 7.4 and rinsed
603 4 times in 0.1 M phosphate buffer pH 7.2 containing 0.02 M glycine. Embryos were post-fixed in
604 2% osmium tetroxide for 1 hour in the dark, rinsed 3 times in dH_2O, stained en bloc in 1% uranyl

605 acetate for 1 hour in the dark, and rinsed 3 times in dH_2O. Samples were dehydrated in a series
606 of ethanol and then propylene oxide twice. Embryos were then infiltrated in propylene oxide:
607 Epon resin series and embedded in Epon at 60ºC for 24 hours. Semi-thin sections were
608 performed followed by Toluidine Blue staining to obtain a salivary gland section. Ultra-thin
609 sections for TEM were cut on a Leica EM UC7 microtome. TEM sections were mounted on
610 carbon-coated copper grids (EMS FCF-150-CU), stained with 2% uranyl acetate and Reynolds
611 lead citrate, and the ultra-thin sections were viewed on a JEOL JEM-1400, 120kV transmission
612 electron microscope and imaged with a Gatan digital camera. Sections from at least five
613 independent embryos were analyzed for wild type and *Papss* mutants.

614

Figures and Figure Legends
Figure 1

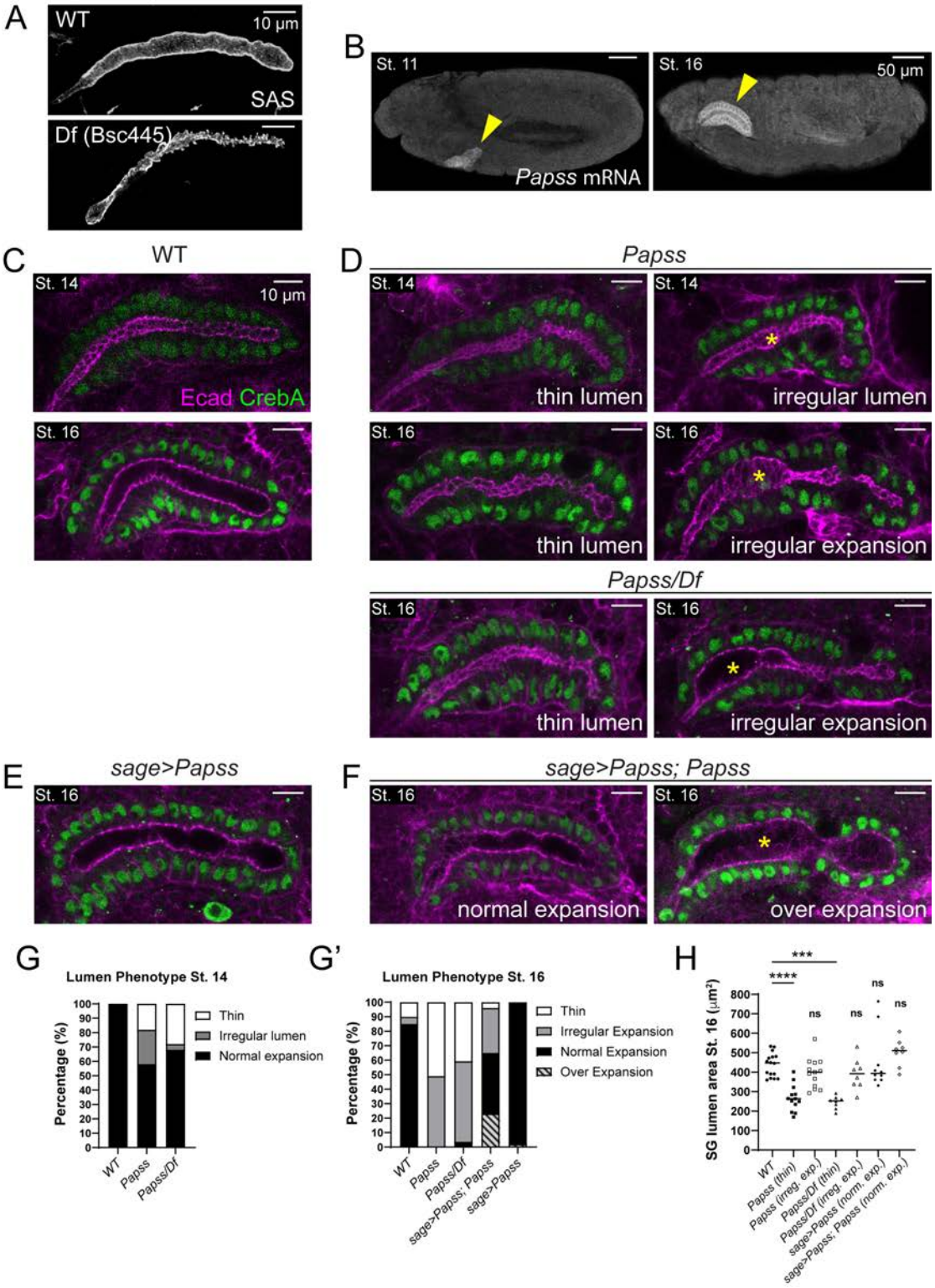

Figure 1. *Papss* mutants show defects in SG lumen expansion. (A) Confocal images of stage 16 SGs immunostained for Stranded at Second (SAS). (B) Confocal image of in situ hybridization for an antisense probe to *Papss* mRNA in stage 11 and 16 embryos. (C-F) Confocal images of stage 14 and stage 16 SGs immunostained for Ecad and CrebA. Yellow asterisks indicate regions of irregular, non-uniform expansion (C) or over-expansion (F) of the SG lumen. (G, G') Quantification of the percentage of embryos with different SG lumen phenotypes for stage 14 (G) and 16 (G') embryos. [(G; n=42 WT; n=38 *Papss*; n=25 *Papss/Df*), (G'; n=40 WT; n=41 *Papss*; n=27 *Papss*/*Df*; n=26 *sage>Papss; Papss*; n=43 *sage>Papss*)]. (H) Quantification of SG lumen area. (n=16 WT; n=13 *Papss* with a thin lumen; n=11 *Papss* with an irregularly expanded lumen; n=8 *Papss/Df* with a thin lumen; n=8 *Papss/Df* with a irregularly expanded lumen; n=10 *sage>Papss* with a normally expanded lumen; n=8 *sage>Papss; Papss* with a normally expanded lumen). Kruskal-Wallis ANOVA test (***, $p<0.001$; ****, $p<0.0001$; ns, non-significant). Horizontal lines indicate mean values.

Figure 2

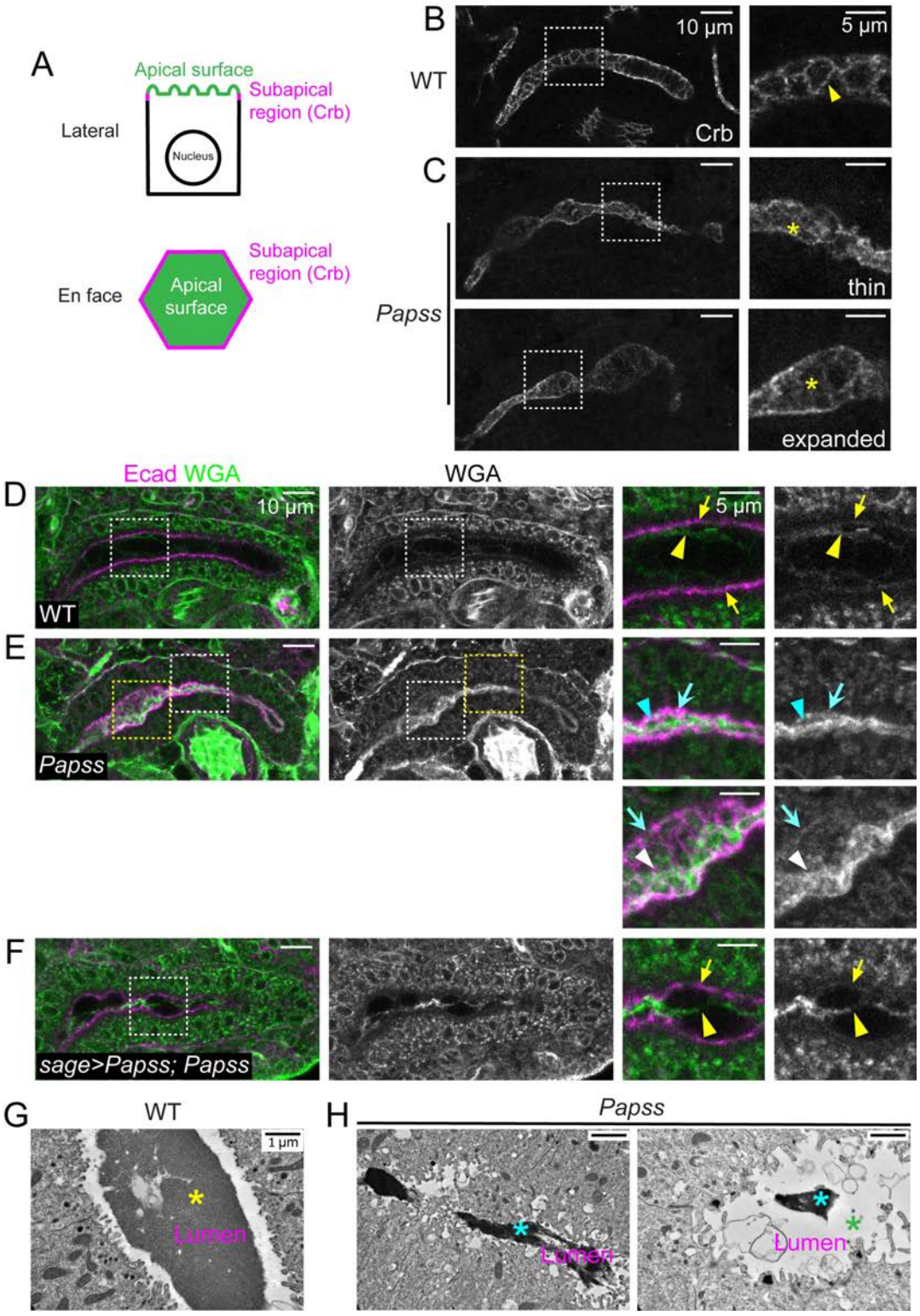
A
Apical surface
Subapical region (Crb)
Lateral
Nucleus
Subapical region (Crb)
En face
Apical surface
B
WT
10 µm
5 µm
Crb
C
Papss
thin
expanded
Ecad WGA
WGA
D
10 µm
5 µm
WT
E
Papss
F
sage>Papss; Papss
G
WT
1 µm
Lumen
H
Papss
Lumen
Lumen

Figure 2. Mutations in *Papss* result in mislocalized Crb and disruption of the aECM architecture. (A) Cartoon of SG epithelial cells showing the subcellular localization of Crb from lateral and en face views. (B-C) Confocal images of stage 16 SGs immunostained for Crb. Magnified images are shown for boxed regions. Arrowhead in B, Crb localizes to the subapical region in WT SG cells. Asterisks in C, Crb mislocalizes to the apical surface region of SG cells in *Papss* mutants, both in thin and expanded regions of the gland. (D-F) Confocal images of stage 16 SGs stained for Ecad antibody and wheat germ agglutinin (WGA). Magnified images are shown for boxed regions. Arrows, WGA localization at the apical membrane in WT (yellow) and *Papss* mutant (cyan) SGs. Yellow arrowheads in D, WGA localizes as a filament in the lumen of WT SG. Cyan arrowheads in E, WGA localizes as a highly condensed structure in the thin luminal region of *Papss* SG. White arrowheads, WGA localizes as a condensed, filamentous structure in the expanded luminal region of the *Papss* mutant SG. Yellow arrowheads in F, WGA localizes as a mildly condensed filament in the lumen of the *sage>Papss; Papss* SG. (G, H) TEM images of stage 15 SGs. Yellow asterisk in G, electron-dense luminal material in WT SG. Cyan asterisks in H, condensed electron-dense luminal material in the *Papss* mutant SG. Green asterisk, large luminal area lacking electron-dense material in the *Papss* mutant SG.

Figure 3

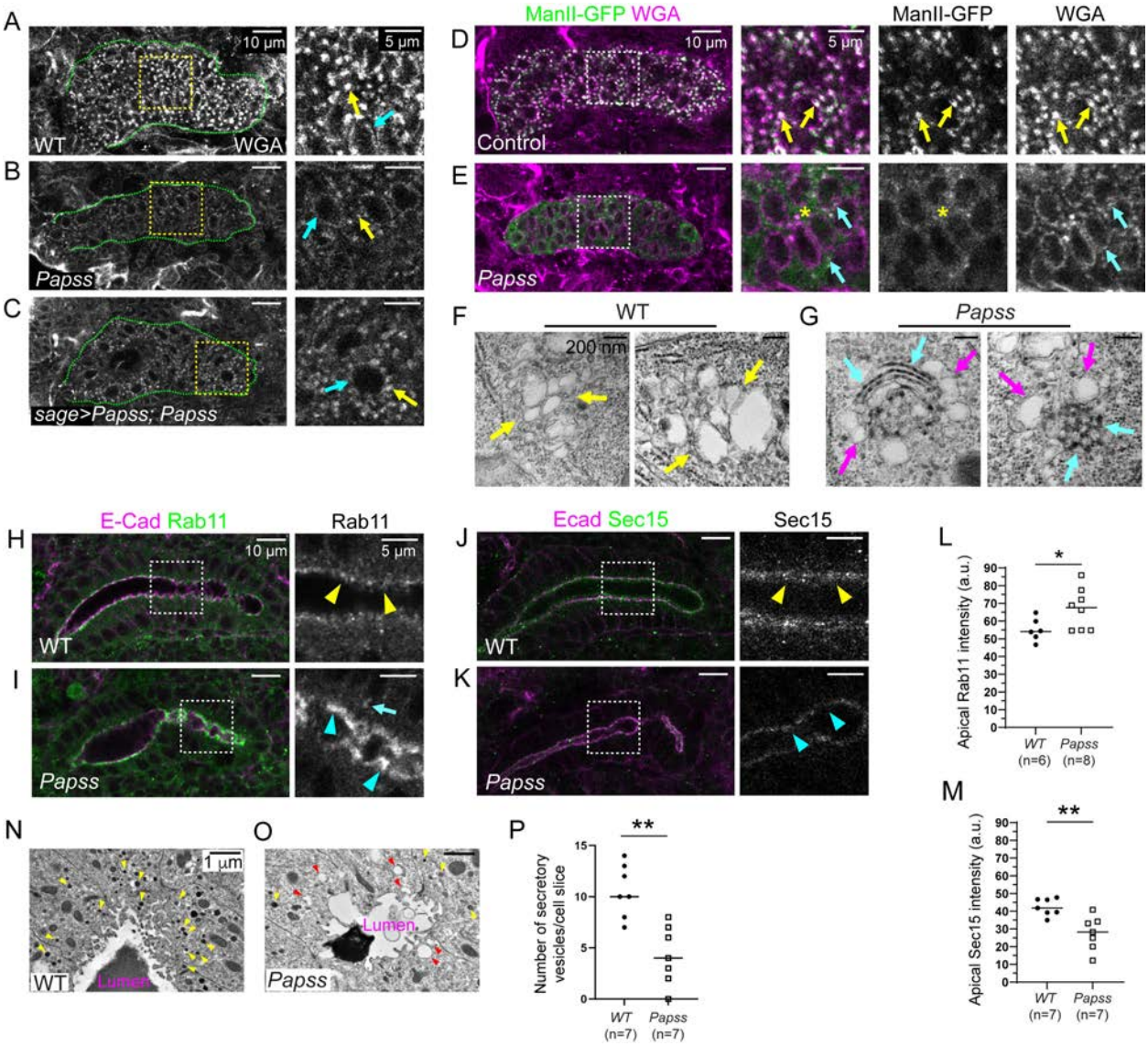

Figure 3. *Papss* mutants show defects in intracellular trafficking. (A-C) Confocal images of stage 16 SGs stained for WGA. Magnified images are shown for boxed regions. Green lines mark the basal boundary of SGs. Yellow arrows, WGA signals as cytoplasmic puncta. Cyan arrows, WGA localized to the nuclear envelope. (D, E) Confocal images of stage 16 SGs stained for GFP (for ManII-GFP) and WGA. Magnified images are shown for boxed regions. Yellow arrows in F, ManII-GFP and WGA puncta colocalize in WT SG. Asterisks in G, ManII-GFP signals are dispersed in the cytoplasm in *Papss* mutants. Cyan arrows in G, ManII-GFP and

WGA show little colocalization in the *Papss* SG. (F, G) TEM images of Golgi. Yellow arrows in F, Golgi structures in WT SG cells. Magenta arrows in G, Golgi structures in the *Papss* SG. Cyan arrows in G, electron-dense structures in the Golgi in *Papss* mutant SG cells. (H, I) Confocal images of stage 16 SGs immunostained for Rab11 and Ecad. Magnified images are shown for boxed regions. Rab11 signals at the apical membrane are increased in *Papss* mutants (cyan arrowheads in I) compared to WT (yellow arrowheads in H), with occasional large punctate signals mislocalized to the basolateral domain (cyan arrow in I). (J, K) Stage 16 SGs immunostained for Sec15 and Ecad. Compared to strong apical Sec15 signals in the WT SG (yellow arrowheads in J), Sec15 signals are reduced in *Papss* mutants (cyan arrowheads in K). (L, M) Quantification of the intensity of Rab11 (L) and Sec15 (M) at the apical membrane regions in WT and *Papss* mutant SGs. Welch's t-test (**, $p<0.05$). Horizontal lines indicate mean values. (N, O) TEM images for the apical region of SG cells. Yellow arrowheads, electro-dense vesicles. Red arrowheads, empty, larger vesicle-like structures. (P) Quantification of the vesicle numbers per cell slice. Welch's t-test (**, $p<0.05$). Horizontal lines indicate mean values.

Figure 4

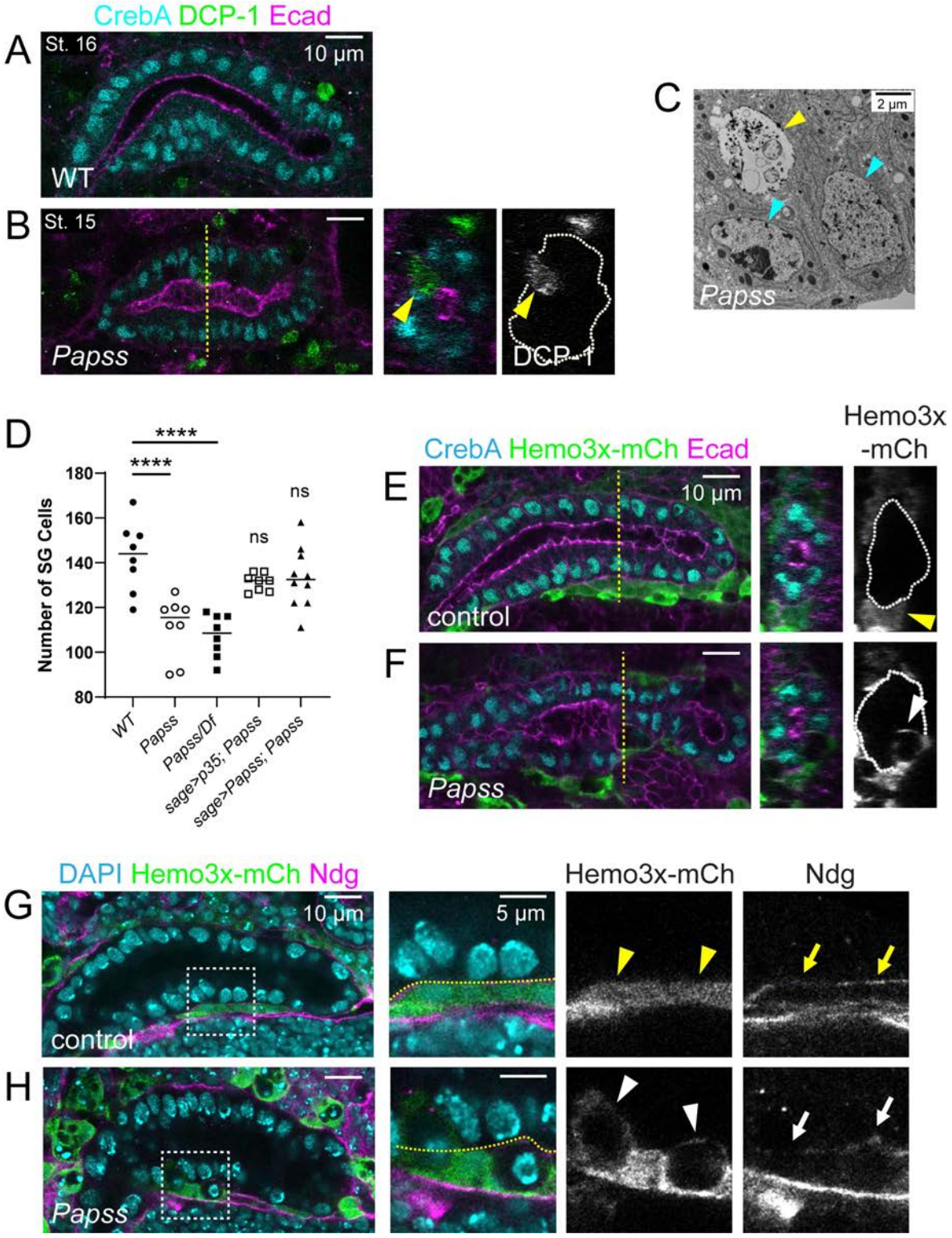
CrebA DCP-1 Ecad
A
St. 16
10 µm
WT
B
St. 15
Papss
DCP-1
C
2 µm
Papss
D
****
****
ns
ns
Number of SG Cells
180
160
140
120
100
80
WT
Papss
Papss/Df
sage>p35; Papss
sage>Papss; Papss
CrebA Hemo3x-mCh Ecad
Hemo3x -mCh
E
10 µm
control
F
Papss
DAPI Hemo3x-mCh Ndg
Hemo3x-mCh
Ndg
G
10 µm
5 µm
control
H
Papss

Figure 4. *Papss* mutants show premature SG cell death. (A, B) Confocal images of stage 16 SGs immunostained for CrebA, DCP-1 and Ecad. Cross-sectional images are shown for the yellow dashed line in B. Yellow arrowheads, Dcp-1 signal is detected in the SG in *Papss* mutants. White dashed lines, the basal boundary of the SG. (C) TEM image of stage 15 SG cells. Cyan arrows, nuclei of normal living cells. Yellow arrow, nucleus of a dying cell. (D) Quantification of the number of SG cells. (n=10 WT; n=10 *Papss*; n=8 *Papss*/*Df*; n=8 *sage>p35; Papss*; n=10 *sage>Papss; Papss*). One way ANOVA test (****, $p<0.0001$; ns, non-significant). (E, F) Confocal images of stage 16 SGs immunostained for CrebA, Ecad, and mCherry (for Hemo3x-mCh). Cross-section images are shown for the yellow dashed lines. White dashed lines, the basal boundary of the SG. Yellow arrowhead in E, hemocyte signals outside of the control SG. White arrowhead in F, hemocyte signals are present inside the SG in *Papss* mutants. (G, H) Stage 16 SGs immunostained for DAPI, mCherry, and Ndg. Magnified views are shown for boxed regions. Yellow dashed lines, the basal boundary of the SG. (G) Hemocytes are found outside of the SG in WT (yellow arrowheads), with Ndg forming a barrier at the basal boundary of the SG (yellow arrows). (H) Hemocytes invade the SG epithelia in *Papss* mutants (white arrowheads), where Ndg signals are irregular or absent (white arrows).

Figure 5

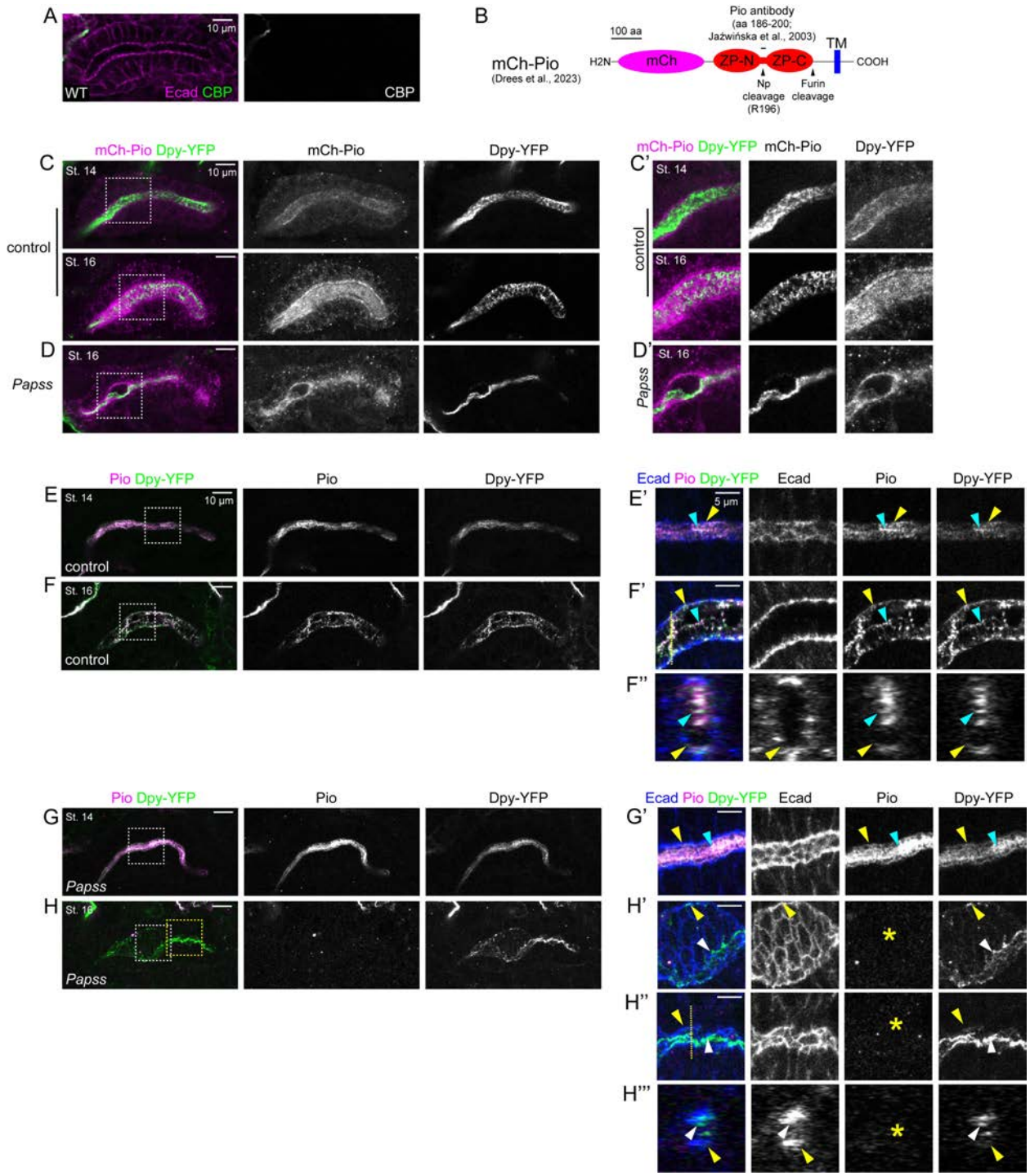

Figure 5. Loss of Papss disrupts the localization of Dpy and Pio in the aECM. (A) Confocal images of stage 16 SGs stained for a chitin-binding protein (CBP) and Ecad. (B) Cartoon for the mCh-Pio fusion protein showing the region for the antibody and protease cleavage sites. (C, D)

Confocal images of stage 14 and stage 16 SGs immunostained for mCh (for mCh-Pio) and GFP (for Dpy-YFP). (E-H’’’) Confocal images of stage 14 and stage 16 SGs immunostained for Pio, GFP, and Ecad. Magnified images of boxed regions in E-H and shown in E’-H’’. F’’ and H’’’ are cross-sectional images of the SG lumen for regions indicated by white lines F’ and H’’. Yellow arrowheads, Pio and Dpy localized to the apical membrane. Cyan arrowheads, Dpy and Pio localized to the SG lumen. Note a higher proportion of Dpy and Pio localized to the lumen in the *Papss* mutant SG at stage 14 (cyan arrowheads in G’). White arrowheads in H’-H’’’, Dpy accumulates towards one side of the lumen in the stage 16 *Papss* SG. Yellow asterisks, Pio is absent from the lumen at stage 16 in the *Papss* SG.

Figure 6

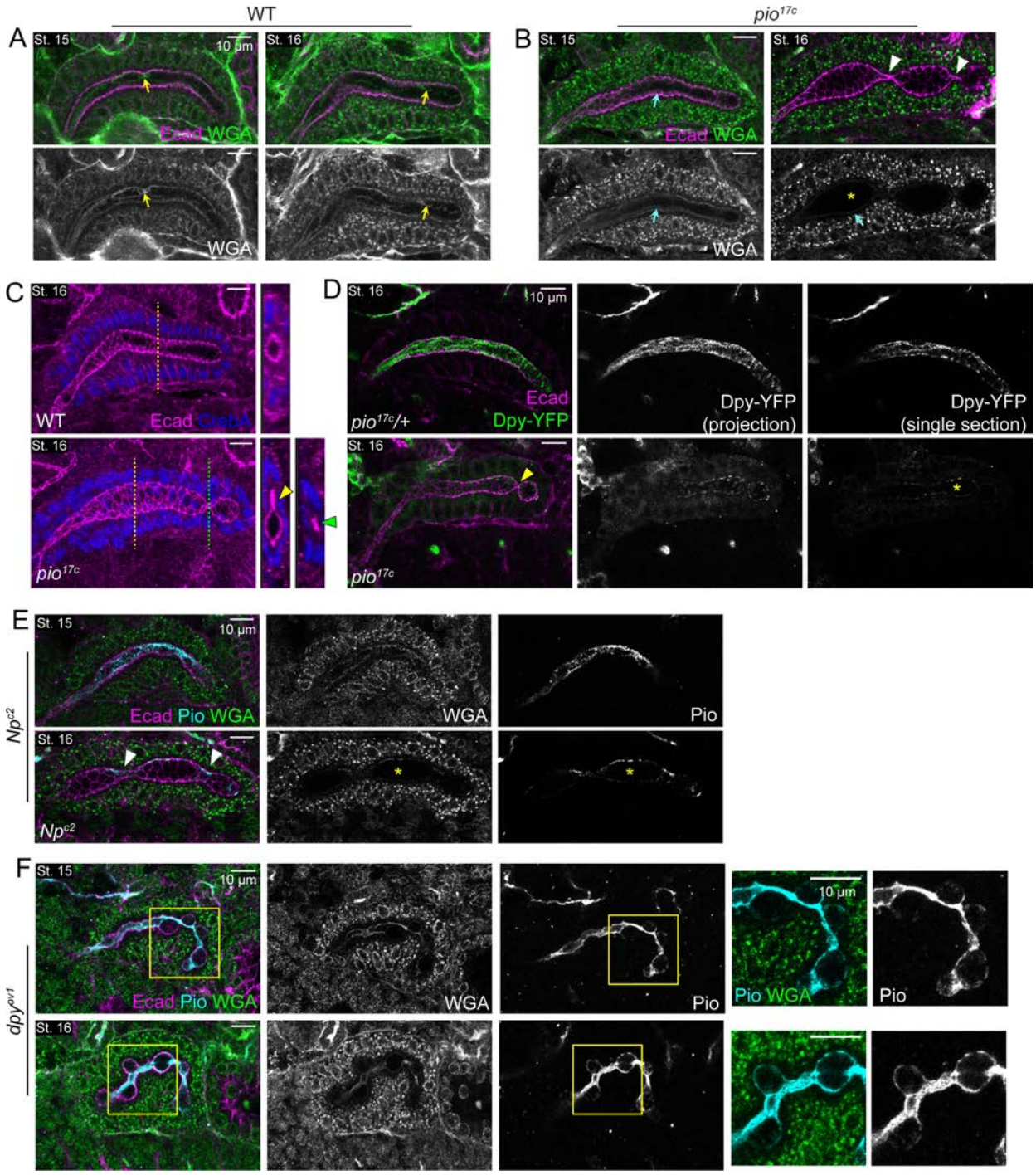

Figure 6. Pio is essential for uniform SG lumen diameter by maintaining Dpy in the lumen. (A, B) Confocal images of SGs at stages 13-16 stained for WGA and Ecad. Yellow arrowheads in A, filamentous luminal WGA signals. Cyan arrowheads in B, WGA signals at the apical

membrane. Yellow asterisks, loss of lumina WGA signals. White arrowheads, constricted lumen. (C) Confocal images of stage 16 SGs immunostained for Ecad and CrebA. Cross sectional images for the yellow and green dotted lines are shown on the right. Yellow arrowhead, flat protrusion of the lumen. Green arrowhead, constricted lumen. (D) Confocal images of stage 16 SGs stained for Ecad and GFP (for Dpy-YFP). Projection images contain merged z-sections, from the apical surface of the SG cells to midway through the SG. Single section, one z-section at the approximate midpoint of the lumen width. Yellow arrowhead, area of constricted lumen. Yellow asterisk, area within the lumen with no Dpy-YFP signals. (E) Confocal images of SGs at stages 15 and 16 stained for Ecad, Pio and WGA. WGA and Pio images are obtained from single z-sections. White arrowheads, area of constricted lumen. Yellow asterisks, no luminal Pio signals. (F) Confocal images of SGs at stages 14-16 stained for Ecad, WGA and Pio. Higher magnification of the yellow boxed regions is shown on the right.

Sup. Fig. S1

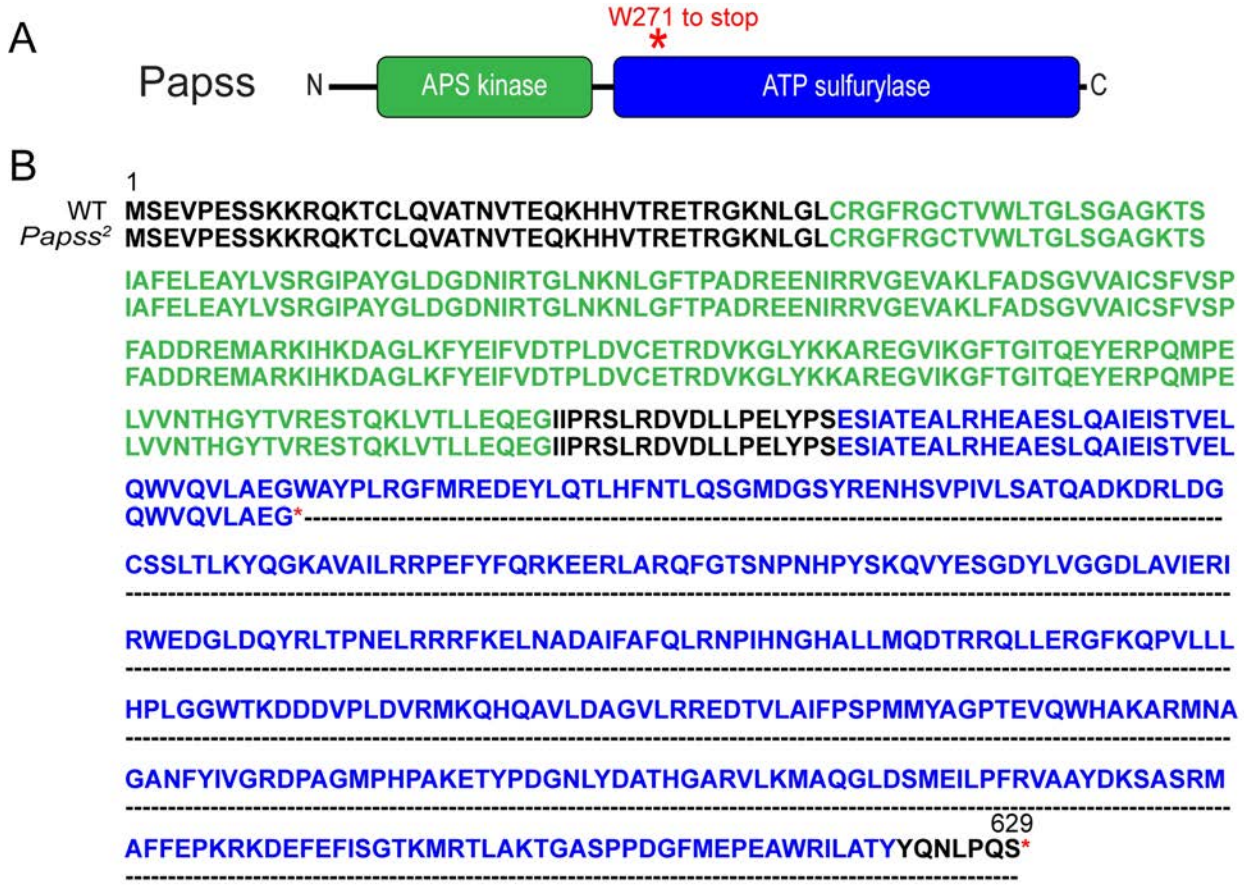

Sup. Fig. S1. *Papss* mutants encode a stop codon in the ATP sulfurylase domain. (A) Cartoon of the Papss-PA isoform showing the APS kinase and ATP sulfurylase domains. A red asterisk indicates the site of the W271->stop mutation. (B) Amino acid sequences for WT and *Papss*^{2} sequences for the Papss-PA isoform. Green text, residues of the APS kinase domain. Blue text, residues of the ATP sulfurase domain. Red asterisks, stop codon. Note that *Papss*^{2} also has a secondary mutation (G->A) at G79 of the transcript resulting in a silent mutation.

Sup. Fig. S2.

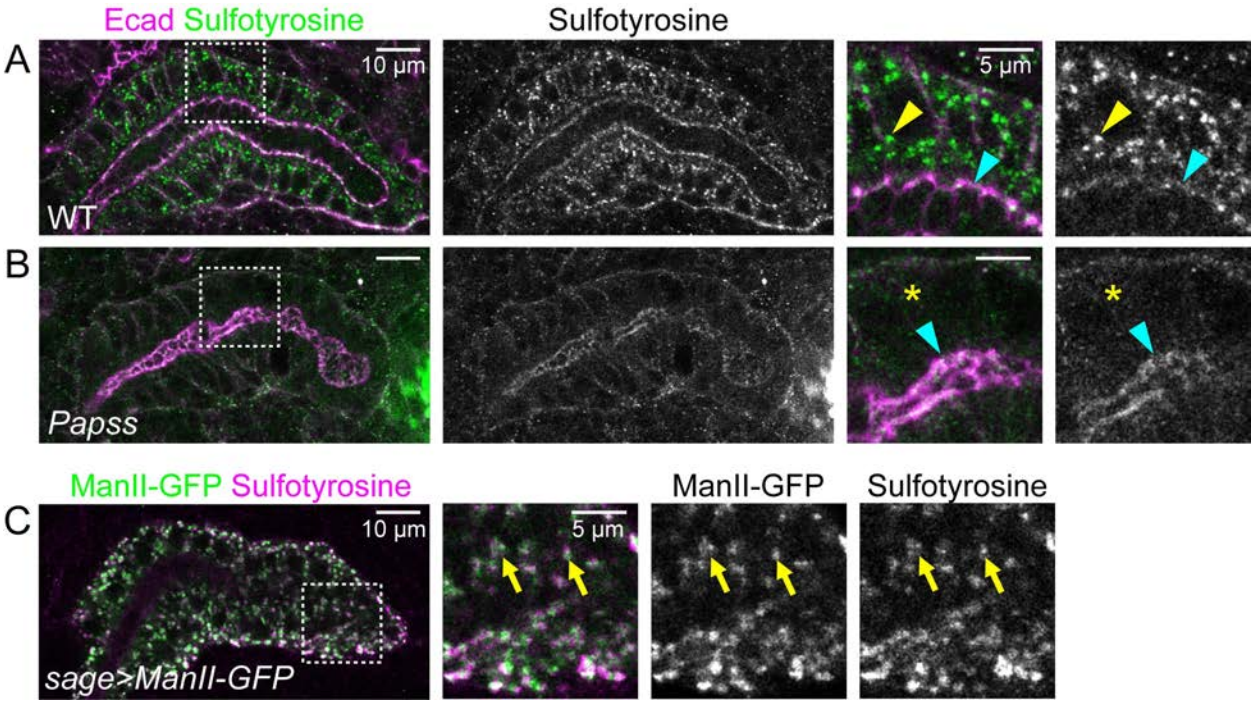

Sup. Fig. S2. Sulfotyrosine signals are reduced in *Papss* mutants. (A, B) Confocal images of SGs immunostained for sulfotyrosine and Ecad in stage 16 WT (A) and *Papss* mutant embryos. Magnified images are shown for boxed regions. Yellow arrowheads, sulfotyrosine-positive cytoplasmic puncta in WT SG cells. Cyan arrowheads, sulfotyrosine at the apical membrane. Asterisks, almost no sulfotyrosine puncta are present in the cytoplasm in *Papss* mutants. (C) Confocal images of stage 16 SGs immunostained for GFP and sulfotyrosine. Arrows, ManII-GFP and Sulfotyrosine puncta co-localize.

Sup. Fig. S3.

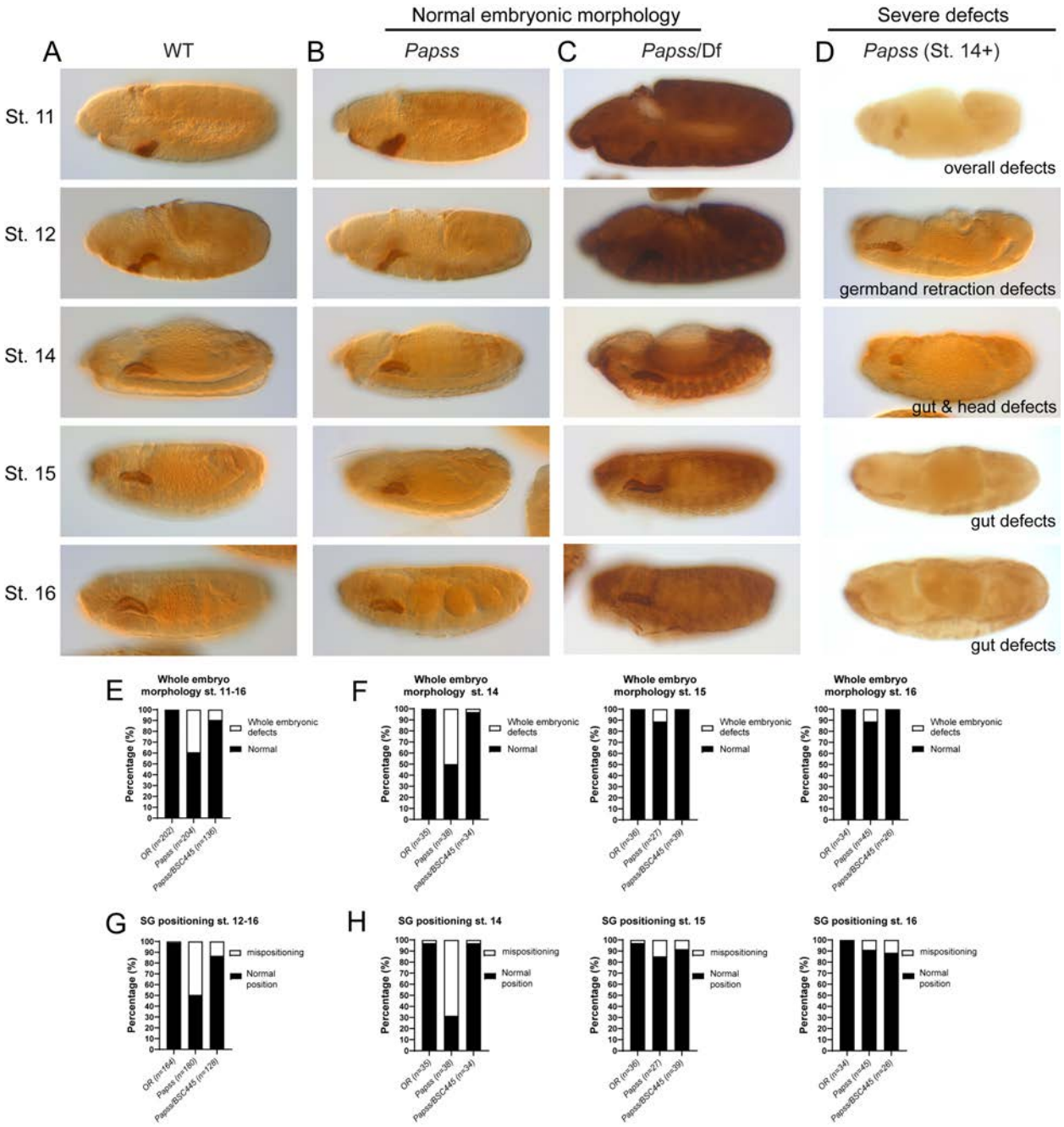

Sup. Fig. S3. Some *Papss* mutant embryos show defective SG formation and whole embryonic defects. (A-D) Confocal images of stages 11-16 embryos immunostained using CrebA. (A) WT. (B) *Papss*, normal embryonic morphology. (C) *Papss*/*Df*, normal embryonic morphology. (D) *Papss*, severely defective whole embryo morphology. (E, F) Quantification of the percentage of embryos with whole embryonic defects. (E) Quantification of combined stages

11-16. (F) Quantification of individual stages for stages 14-16. (G-H) Quantification of the percentage of embryos with SG invagination defects/mispositioned SG. (G) Quantification of combined stages 12-16. (H) Quantification of individual stages for stages 14-16.

Sup. Fig. S4.

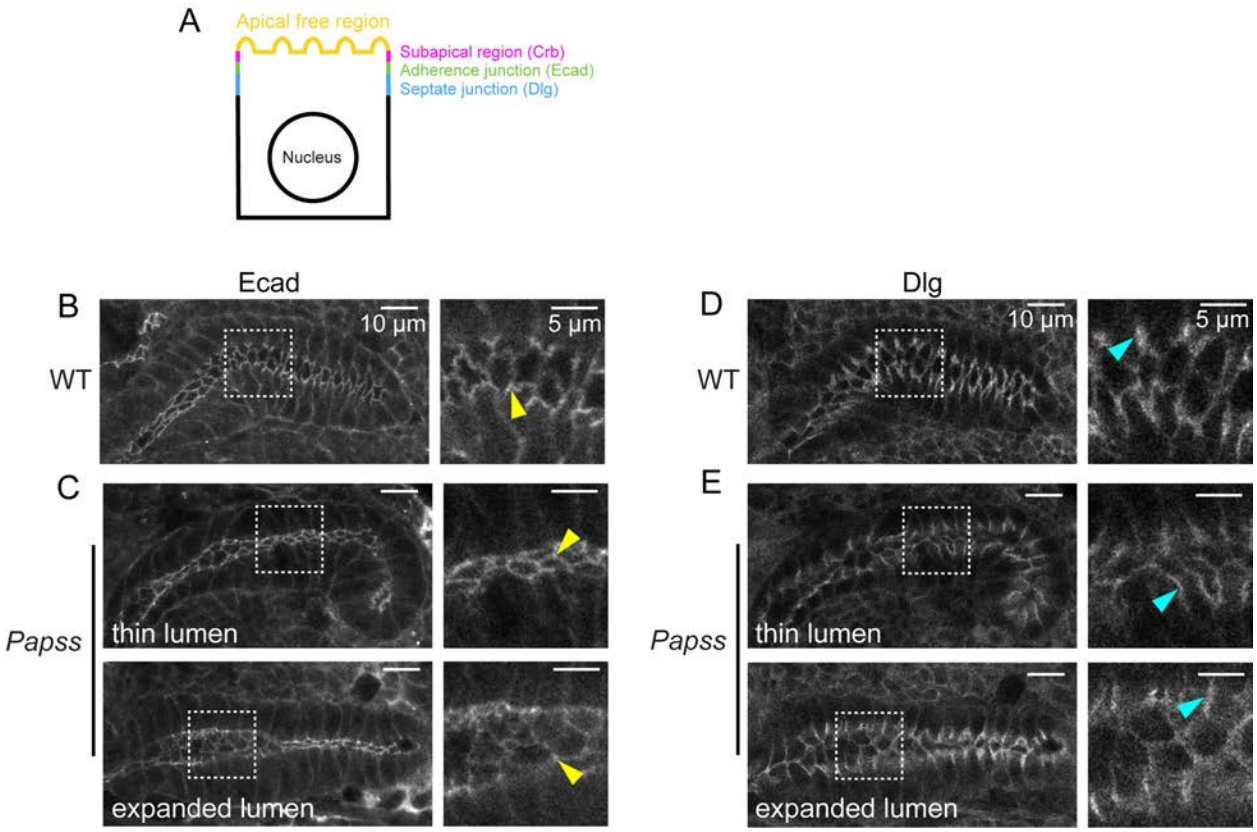

Sup. Fig. S4. Adherens junctions (AJs) and septate junctions (SJs) are intact in *Papss* mutants. (A) Cartoon showing the subapical and junctional regions in the SG epithelial cell from the lateral view and localization of the key protein markers Crb, Ecad, and Dlg. (B, C) Confocal images of stage 16 SGs immunostained for Ecad. Magnified images are shown for boxed regions. Yellow asterisks, localization of Ecad to AJs in both WT (B) and *Papss* mutant (C) SGs. (D, E) Confocal images of stage 16 SGs immunostained for Dlg. Images show the luminal surface view. Cyan asterisks, localization of Dlg at SJs in both WT (D) and *Papss* mutant (E) SGs. SJs in *Papss* mutants occasionally appear slightly longer in the expanded luminal region compared to WT or the thin luminal region of *Papss* mutants, possibly due to stretching of cells with lumen expansion.

Sup. Fig. S5.

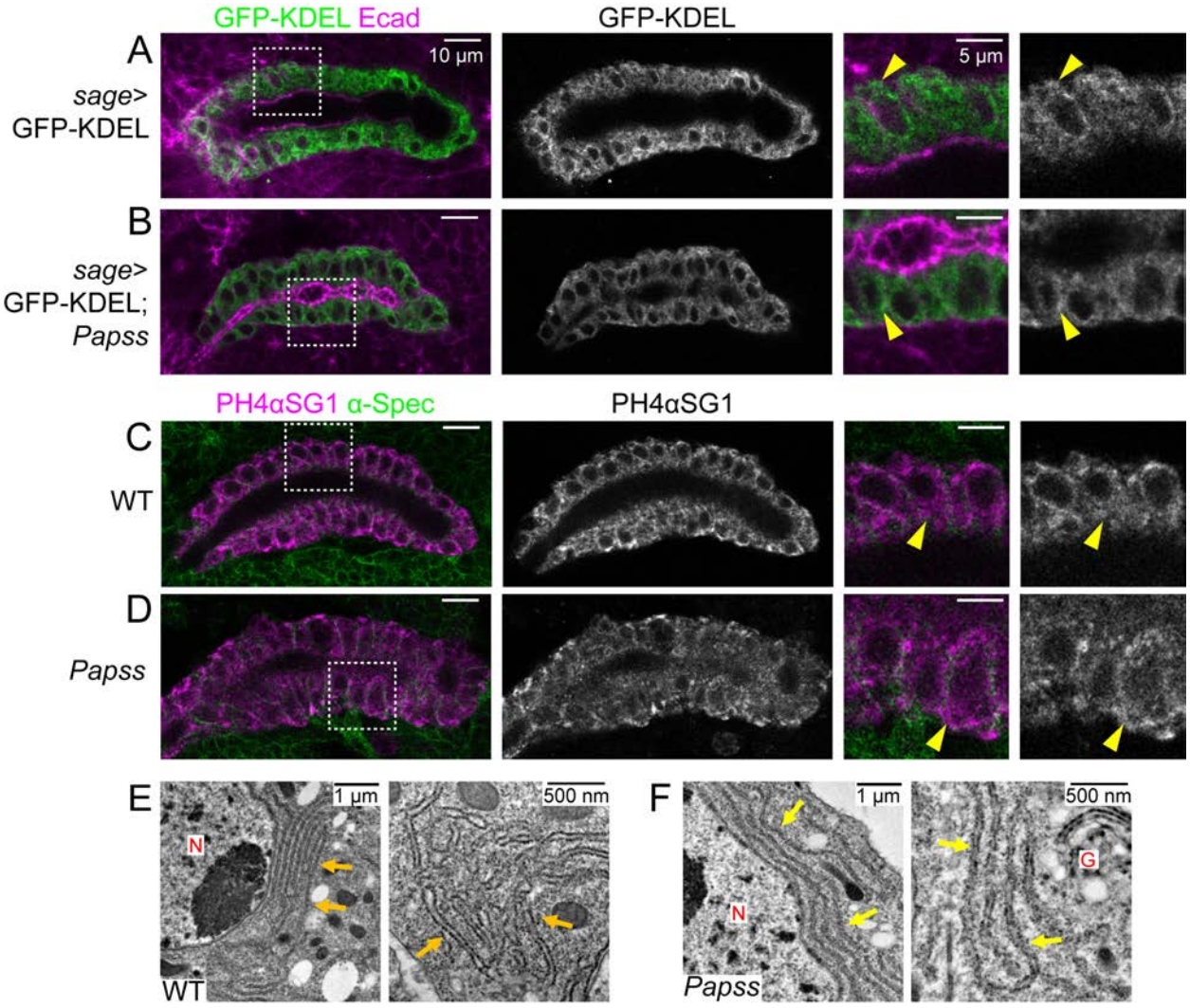

Sup. Fig. S5. The Endoplasmic reticulum is intact in *Papss* mutants. (A, B) Confocal images of stage 16 SGs immunostained for GFP (for GFP-KDEL) and Ecad. Magnified images are shown for boxed regions. Yellow arrowheads, KDEL signals in control (A) and *Papss* mutant (B) SGs. (C, D) Confocal images of stage 16 SGs immunostained for PH4αSG1 and α-Spectrin. Magnified images are shown for boxed regions. Yellow arrows, PH4αSG1 signals in the ER in WT (C) and *Papss* mutant (D) SGs. (E, F) TEM images of SG epithelial cells. N indicates nucleus. G indicates the Golgi. Yellow arrows, ER.

Sup. Fig. S6.

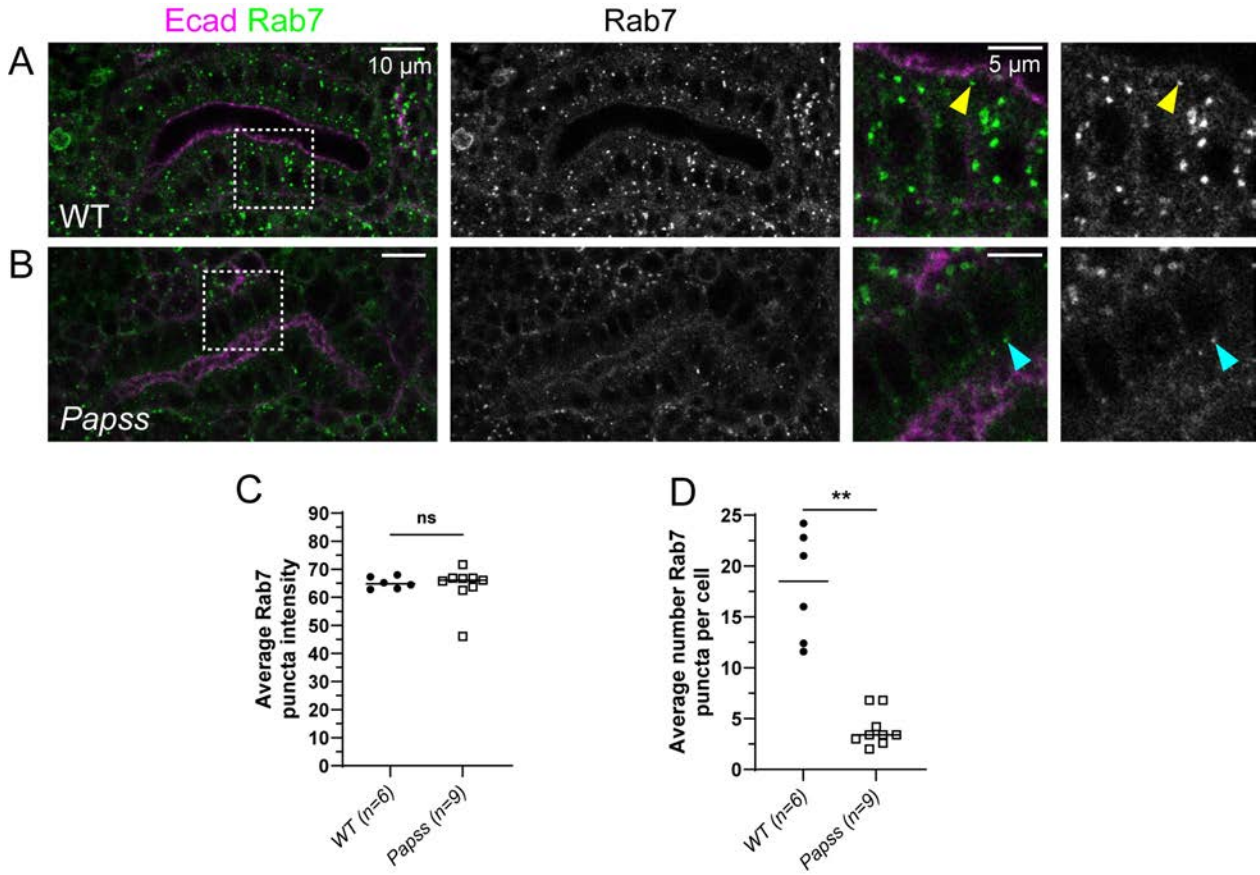

Sup. Fig. S6. Rab7 punctate number is decreased in *Papss* mutants. (A) Confocal images of stage 16 SGs immunostained for Rab7 and Ecad. Magnified images are shown for boxed regions. Yellow arrowheads in A, Rab7 signals in WT. Cyan arrowheads in B, Rab7 puncta are reduced in *Papss* mutants. (B) Quantification for the average mean gray value intensity of Rab7 puncta per sample. (C) Quantification of the average number of Rab7 puncta found in each cell for one sample. (B-C) Welch's t-test (**, $p<0.01$). Horizontal lines indicate mean values.

Sup. Fig. S7.

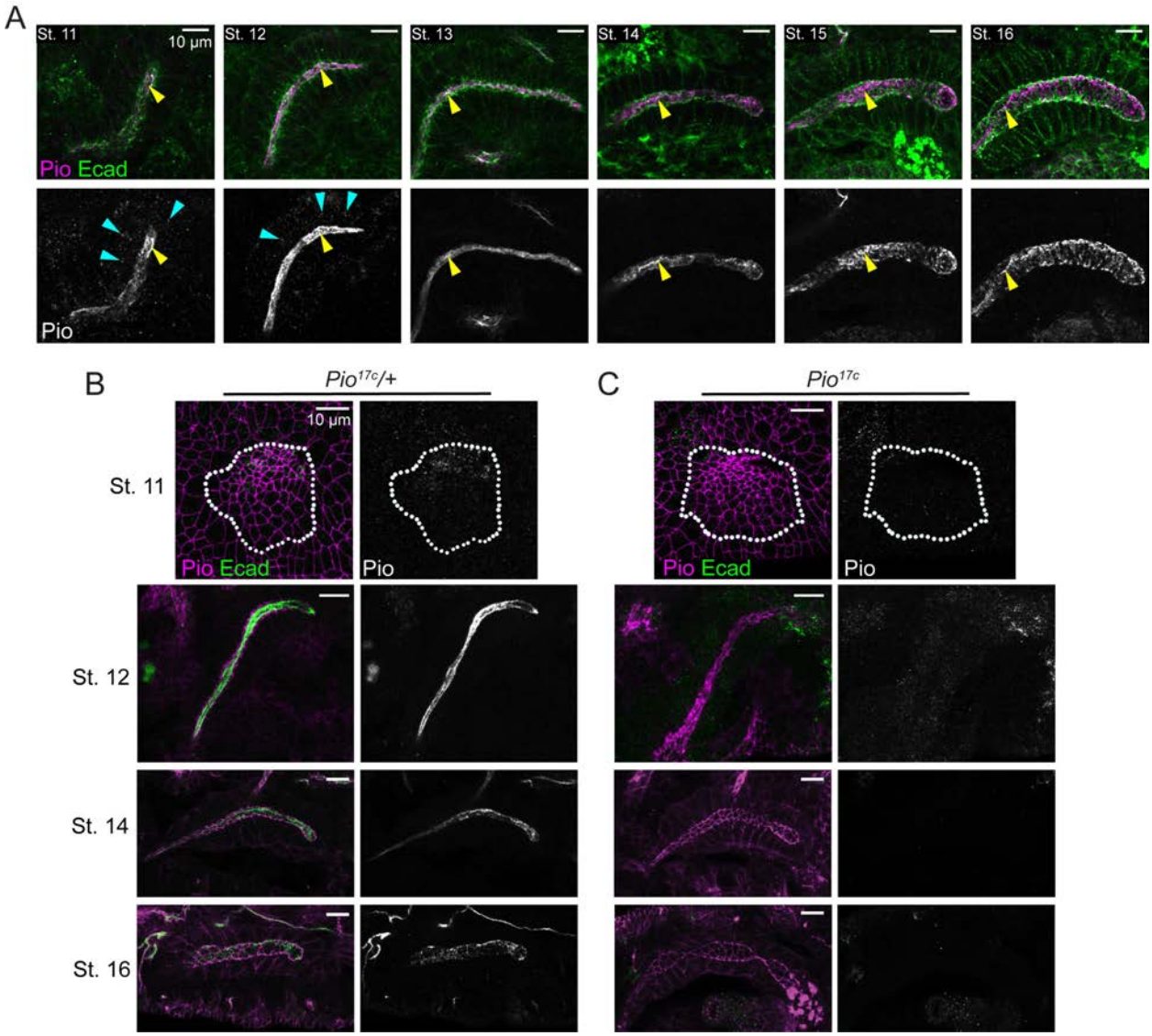

Sup. Fig. S7. Localization of Pio throughout SG development. (A) Confocal images of stage 11-16 SGs immunostained for Pio and Ecad. Yellow arrowheads, Pio localizes to the SG lumen. Cyan arrowheads, Pio signals as cytoplasmic puncta. (B, C) Confocal images of stage 11-16 SGs immunostained for Pio and Ecad. Whereas filamentous luminal Pio signals are shown in control (B), no Pio signals are detected in *pio* null mutants (C). For stage 11, ventral views are shown, with white dotted lines indicating the boundary of the SG placode. Lateral views are shown for other stages.

Sup. Fig. S8.

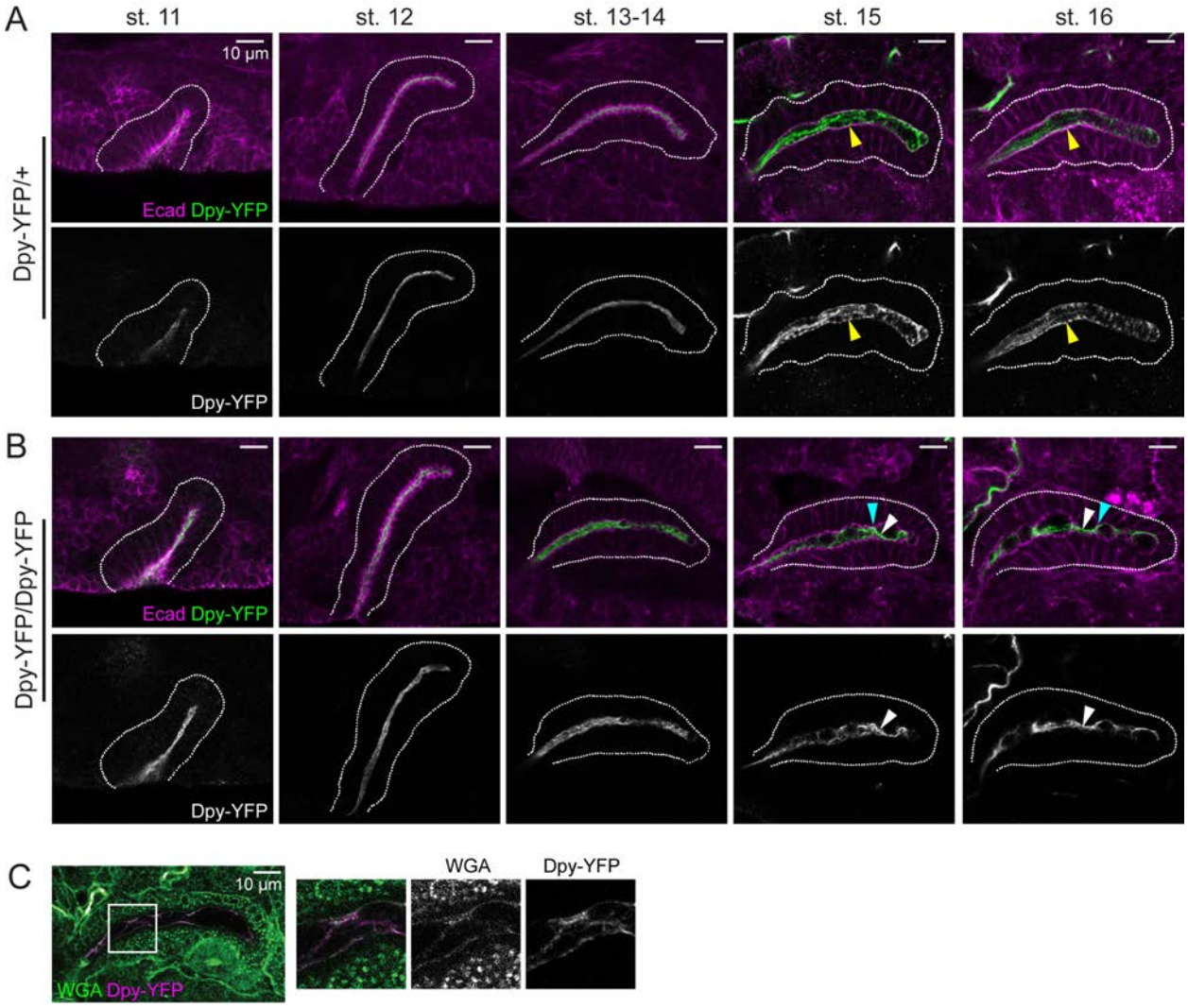

Sup. Fig. S8. Dpy localization through SG morphogenesis. (A-B) Confocal images of stage 11-16 SGs immunostained using GFP and Ecad. White dotted lines indicate the basal boundary of SGs. (A) Dpy-YFP heterozygous samples. Yellow arrowhead, Dpy is localized in the SG lumen in an organized, filametous meshwork in Dpy-YFP/+. (B) Dpy-YFP homozygous samples. Cyan arrowheads, the SG lumen shows sites of constriction in Dpy-YFP/Dpy-YFP. White arrowheads, Dpy organization is irregular in the SG lumen of Dpy-YFP homozygous embryos. (C) Stage 16 Dpy-YFP/+ SG stained for WGA. Luminal filamentous Dpy-YFP signals colocalize with WGA signals. Magnified images are shown for the boxed region.

Sup. Fig. S9.

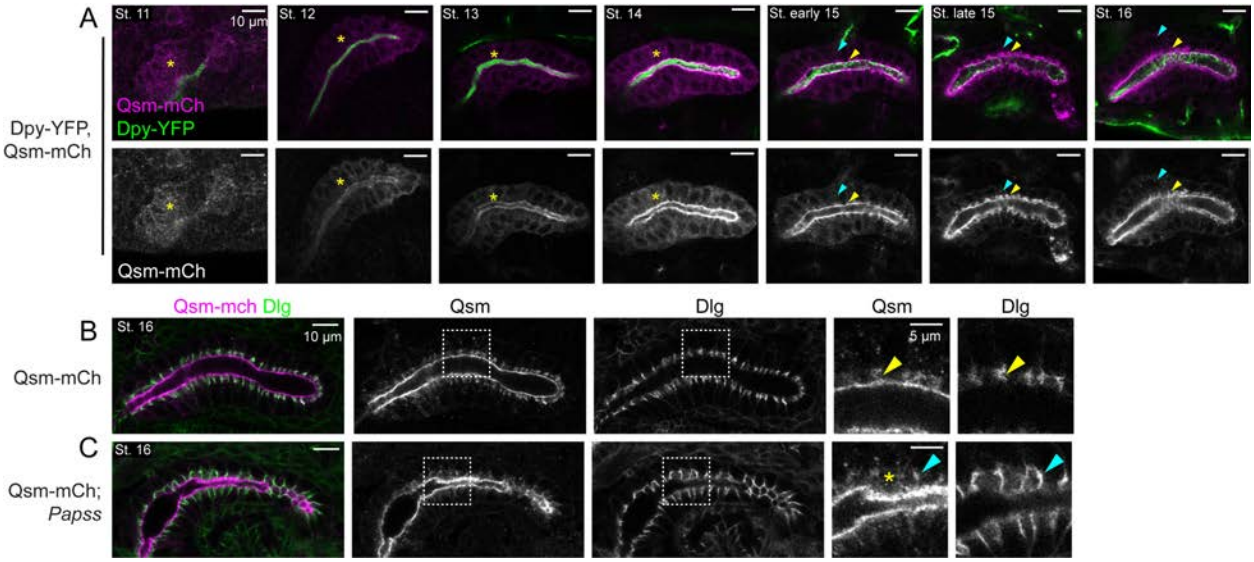

Sup. Fig. S9. Qsm localization patterns are not significantly affected in *Papss* mutants. (A) Confocal images of stage 11-16 SGs immunostained for GFP (for Dpy-YFP) and mCh (for Qsm-mCh). Yellow asterisks, Qsm signals in the cytoplasm of SG cells. Yellow arrowheads, Qsm shows increased localization at the apical membrane and septate junctions in the late stage SG. Cyan arrowheads, Qsm-mCh-positive puncta in the cytoplasm increase at early stage 15 in the SG. (B, C) Confocal images of stage 16 SGs immunostained for mCh and Dlg. Enlarged images are shown for boxed regions. Qsm partially colocalizes with Dlg in control (yellow arrowheads) and *Papss* mutant (cyan arrowheads) SGs. Yellow asterisks, dispersed Qsm signals near the apical membrane.

Sup. Fig. S10.

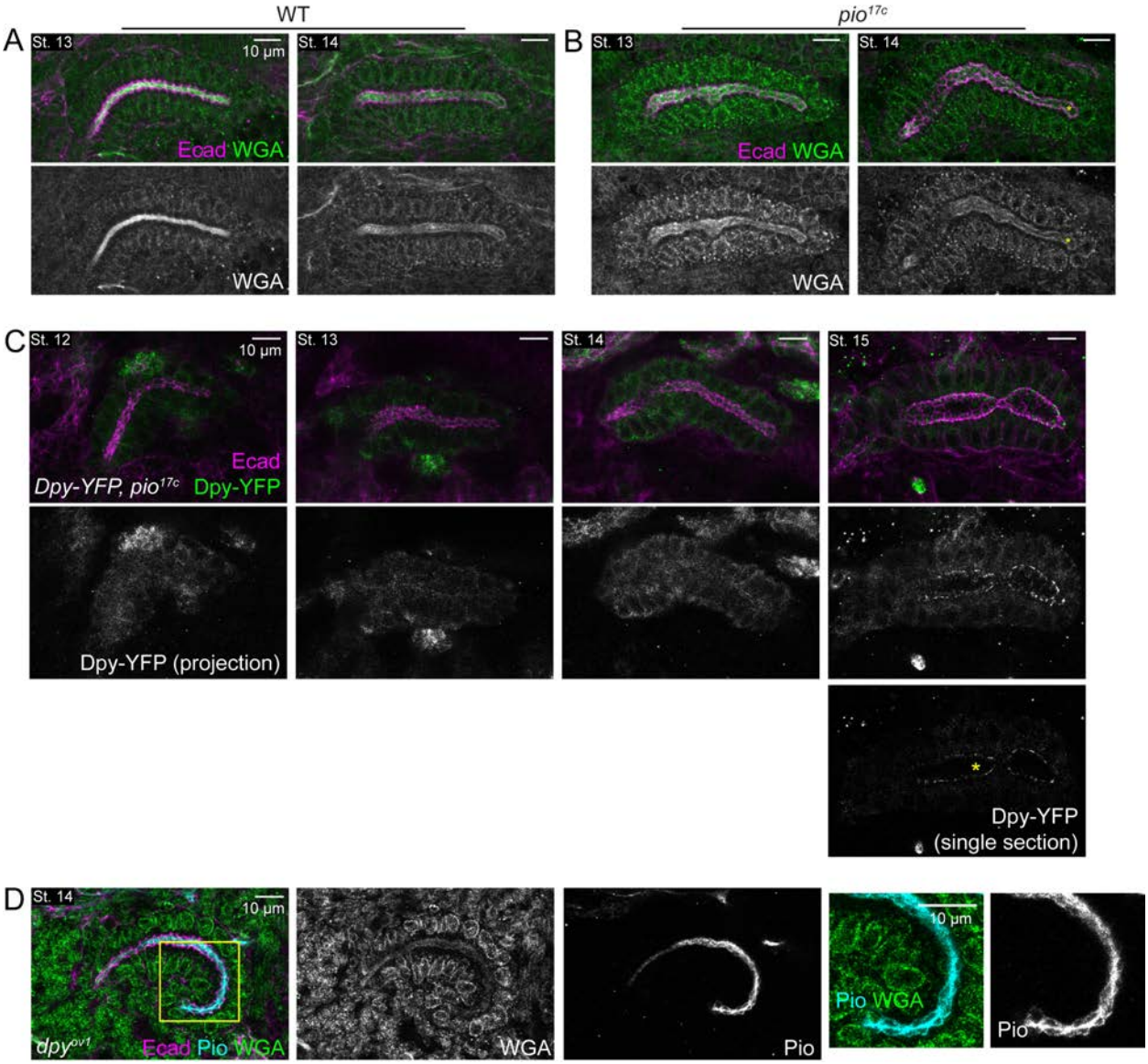

Sup. Fig. S10. Loss of *pio* affects Dpy localization patterns and vice versa in the SG. (A, B) Confocal images of the SG immunolabeled for Ecad and WGA at stages 13 and 14 in WT (A) and *pio* mutant (B) embryos. (C) Confocal images of *pio* mutant SGs from stages 12-15 immunostained for Ecad and GFP (for Dpy-YFP). Projection images contain merged z-sections, from the apical surface of the SG cells to midway through the SG. Single section for stage 16, one z-section at the approximate midpoint of the lumen width. (D) Confocal images of *dpy* mutant SG at stage 14 immunostained for Ecad, Pio and WGA. Yellow boxes, area of higher magnification.

Acknowledgements

We thank the members of the Chung laboratory for their comments and suggestions. We thank M. Behr, S. Hayashi, the Bloomington stock center (NIH P40OD018537), and the Kyoto *Drosophila* stock center at Kyoto Institute of Technology for fly stocks. We thank M. Affolter for the Pio antibody. Many antibodies were obtained from the Developmental Studies Hybridoma Bank, created by the NICHD of the NIH and maintained at The University of Iowa, Department of Biology, Iowa City, IA 52242. cDNAs for *Papss* were obtained from the *Drosophila* Genomics Resource Center (NIH 2P40OD010949). This work was supported by the National Science Foundation (MCB 2141387) to SC.

Table S1. A targeted Df screen revealed Papss as a key enzyme for SG lumen expansion.

SG-upregulated enzymes	Predicted roles	Df lines tested	SG lumen shape
CG17633	Metallocarboxypeptidase	Exel6024	Disrupted embryo morphology
CG30283	Serine-type endopeptidase	Exel6076	Disrupted embryo morphology
Papss	PAPS synthetase	Bsc445	Thin SG lumen with apical protrusions
PH4αSG1/SG2	Prolyl 4-hydroxylase	Exel6216	Non-uniform lumen diameter
CG16758	Purine nucleotide phosphorylase	Bsc116	Non-uniform lumen diameter
CG8708	N-acetylgalactosaminide β-1,3-galactosyltransferase	Exel7095	Irregular apical membrane
CG7920	Acetate CoA-transferase	Bsc620	Irregular apical membrane
Pgant6	Polypeptide N-acetylgalactosaminyltransferase	Exel6091	Irregular apical membrane
GlcAT-P	Glucuronosyltransferase	Bsc817	Irregular apical membrane
CG34290	Serine-type endopeptidase	Bsc638	Irregular apical membrane
Peroxidasin	Bromide peroxidase	Bsc119	Irregular apical membrane
ScsβG	Succinyl Co-A synthetase β subunit	Bsc387	Short and rounded SG

Table S2. Fly strains used

Fly strain	**Sources and References**	**RRID**
Oregon R (wild type)		
sage-Gal4	Chung et al., 2009	
Papss^{2}	Bloomington Stock Center	BDSC_26171
UAS-p35	Bloomington Stock Center	BDSC_5072
UAS-Papss-PD	This work	
UAS-Papss-PE	This work	
Dpy-YFP	Kyoto stock center	DGGR_115238
SprHemo3x-mCherry	Gyoergy et al., 2018	BDSC_78358
Dp-YFP. Qsm-mCh	Chu & Hayashi, 2021	
Qsm-mCh	Chu & Hayashi, 2021	
Dpy-YFP, mCh-Pio	Drees et al., 2023	
UAS-ManII-GFP	Bloomington stock center	BDSC_65248
UAS-GFP-KDEL	Bloomington stock center	BDSC_9898
pio^{17c}	Drees et al., 2023	
dpy^{ov1}	Bloomington stock center	BDSC_276
Np^{C2}	Drees et al., 2023	

Table S3. Antibodies Used

Antibody	Source	RRID	Dilution
α-Ecad (rat)	DSHB (DCAD2)	AB_528120	1:50
α-CrebA (rat)	Andrew lab (John Hopkins University); re-made in this study		1:3,000
α-CrebA (rabbit)	Andrew lab (John Hopkins University)	AB_10805295	1:5,000
α-CrebA (guinea pig)	This study		1:5,000
α-GFP (mouse)	Invitrogen (A11120)	AB_221568	1:500
α-GFP (chicken)	Invitrogen (A10262)	AB_2534023	1:1,000
α-RFP (rabbit)	Invitrogen (R10367)	AB_10563941	1: 2,000
α-β-galactosidase (rabbit)	Invitrogen (A11132)	AB_221539	1:500
α-β-galactosidase (mouse)	Invitrogen (MA5-15222)	AB_10980770	1:500
α-mCherry (rat)	Invitrogen (M11217)	AB_2536611	1:1,000
α-mCherry (rabbit)	Invitrogen (PA534974)	AB_2552323	1:1,000
α-DCP-1 (rabbit)	Cell signaling technology (9578)	AB_2721060	1:200
α-Crb (mouse)	DSHB (Cq4)	AB_528181	1:10
α-Rab11 (rabbit)	Andrew lab (John Hopkins University)		1:500
α-Rab7 (mouse)	DSHB (Rab7)	AB_2722471	1:10
α-Sec15 (guinea pig)	Bellen lab (Baylor College of Medicine)		1:2,000
α-α-Spectrin (mouse)	DSHB (3A9)	AB_528473	1:2
α-Discs large (mouse)	DSHB (4F3)	AB_528203	1:500
α-Pio (rabbit)	Jazwinska et al., 2003		1:500

Alexa Fluor 488/568/647-coupled secondary antibodies	Invitrogen		1:500

Uncategorized References

Abrams, E. W., Mihoulides, W. K., & Andrew, D. J. (2006). Fork head and Sage maintain a uniform and patent salivary gland lumen through regulation of two downstream target genes, PH4alphaSG1 and PH4alphaSG2. *Development*, *133*(18), 3517-3527. https://doi.org/10.1242/dev.02525

Ahmad, M., Faiyaz Ul Haque, M., Ahmad, W., Abbas, H., Haque, S., Krakow, D., Rimoin, D. L., Lachman, R. S., & Cohn, D. H. (1998). Distinct, autosomal recessive form of spondyloepimetaphyseal dysplasia segregating in an inbred Pakistani kindred. *Am J Med Genet*, *78*(5), 468-473. https://www.ncbi.nlm.nih.gov/pubmed/9714015

Araujo, S. J., Aslam, H., Tear, G., & Casanova, J. (2005). mummy/cystic encodes an enzyme required for chitin and glycan synthesis, involved in trachea, embryonic cuticle and CNS development--analysis of its role in Drosophila tracheal morphogenesis. *Dev Biol*, *288*(1), 179-193. https://doi.org/10.1016/j.ydbio.2005.09.031

Aumailley, M., Battaglia, C., Mayer, U., Reinhardt, D., Nischt, R., Timpl, R., & Fox, J. W. (1993). Nidogen mediates the formation of ternary complexes of basement membrane components. *Kidney Int*, *43*(1), 7-12. https://doi.org/10.1038/ki.1993.3

Bokel, C., Prokop, A., & Brown, N. H. (2005). Papillote and Piopio: Drosophila ZP-domain proteins required for cell adhesion to the apical extracellular matrix and microtubule organization. *J Cell Sci*, *118*(Pt 3), 633-642. https://doi.org/10.1242/jcs.01619

Bradley, P. L., & Andrew, D. J. (2001). ribbon encodes a novel BTB/POZ protein required for directed cell migration in Drosophila melanogaster. *Development*, *128*(15), 3001-3015. https://doi.org/10.1242/dev.128.15.3001

Bradley, P. L., Myat, M. M., Comeaux, C. A., & Andrew, D. J. (2003). Posterior migration of the salivary gland requires an intact visceral mesoderm and integrin function. *Dev Biol*, *257*(2), 249-262. https://doi.org/10.1016/s0012-1606(03)00103-9

Chandrasekaran, V., & Beckendorf, S. K. (2003). senseless is necessary for the survival of embryonic salivary glands in Drosophila. *Development*, *130*(19), 4719-4728. https://doi.org/10.1242/dev.00677

Chu, W. C., & Hayashi, S. (2021). Mechano-chemical enforcement of tendon apical ECM into nano-filaments during Drosophila flight muscle development. *Curr Biol*, *31*(7), 1366-1378 e1367. https://doi.org/10.1016/j.cub.2021.01.010

Chung, S., & Andrew, D. J. (2014). Cadherin 99C regulates apical expansion and cell rearrangement during epithelial tube elongation. *Development*, *141*(9), 1950-1960. https://doi.org/10.1242/dev.104166

Chung, S., Hanlon, C. D., & Andrew, D. J. (2014). Building and specializing epithelial tubular organs: the Drosophila salivary gland as a model system for revealing how epithelial organs are specified, form and specialize. *Wiley Interdiscip Rev Dev Biol*, *3*(4), 281-300. https://doi.org/10.1002/wdev.140

Chung, S., Kim, S., & Andrew, D. J. (2017). Uncoupling apical constriction from tissue invagination. *Elife*, *6*. https://doi.org/10.7554/eLife.22235

Chung, S., Vining, M. S., Bradley, P. L., Chan, C. C., Wharton, K. A., Jr., & Andrew, D. J. (2009). Serrano (sano) functions with the planar cell polarity genes to control tracheal tube length. *PLoS Genet*, *5*(11), e1000746. https://doi.org/10.1371/journal.pgen.1000746

Cohen, J. D., Bermudez, J. G., Good, M. C., & Sundaram, M. V. (2020). A C. elegans Zona Pellucida domain protein functions via its ZPc domain. *PLoS Genet*, *16*(11), e1009188. https://doi.org/10.1371/journal.pgen.1009188

Cohen, J. D., Sparacio, A. P., Belfi, A. C., Forman-Rubinsky, R., Hall, D. H., Maul-Newby, H., Frand, A. R., & Sundaram, M. V. (2020). A multi-layered and dynamic apical extracellular matrix shapes the vulva lumen in Caenorhabditis elegans. *Elife*, *9*. https://doi.org/10.7554/eLife.57874

Cohen, J. D., & Sundaram, M. V. (2020). C. elegans Apical Extracellular Matrices Shape Epithelia. *J Dev Biol*, *8*(4). https://doi.org/10.3390/jdb8040023

Devine, W. P., Lubarsky, B., Shaw, K., Luschnig, S., Messina, L., & Krasnow, M. A. (2005). Requirement for chitin biosynthesis in epithelial tube morphogenesis. *Proc Natl Acad Sci U S A*, *102*(47), 17014-17019. https://doi.org/10.1073/pnas.0506676102

Dong, B., Miao, G., & Hayashi, S. (2014). A fat body-derived apical extracellular matrix enzyme is transported to the tracheal lumen and is required for tube morphogenesis in Drosophila. *Development*, *141*(21), 4104-4109. https://doi.org/10.1242/dev.109975

Drees, L., Konigsmann, T., Jaspers, M. H. J., Pflanz, R., Riedel, D., & Schuh, R. (2019). Conserved function of the matriptase-prostasin proteolytic cascade during epithelial morphogenesis. *PLoS Genet*, *15*(1), e1007882. https://doi.org/10.1371/journal.pgen.1007882

Drees, L., Schneider, S., Riedel, D., Schuh, R., & Behr, M. (2023). The proteolysis of ZP proteins is essential to control cell membrane structure and integrity of developing tracheal tubes in Drosophila. *Elife*, *12*. https://doi.org/10.7554/eLife.91079

Faiyaz ul Haque, M., King, L. M., Krakow, D., Cantor, R. M., Rusiniak, M. E., Swank, R. T., Superti-Furga, A., Haque, S., Abbas, H., Ahmad, W., Ahmad, M., & Cohn, D. H. (1998). Mutations in orthologous genes in human spondyloepimetaphyseal dysplasia and the brachymorphic mouse. *Nat Genet*, *20*(2), 157-162. https://doi.org/10.1038/2458

Ford-Hutchinson, A. F., Ali, Z., Seerattan, R. A., Cooper, D. M., Hallgrimsson, B., Salo, P. T., & Jirik, F. R. (2005). Degenerative knee joint disease in mice lacking 3'-phosphoadenosine 5'-phosphosulfate synthetase 2 (Papss2) activity: a putative model of human PAPSS2 deficiency-associated arthrosis. *Osteoarthritis Cartilage*, *13*(5), 418-425. https://doi.org/10.1016/j.joca.2004.12.011

Fox, R. M., & Andrew, D. J. (2015). Changes in organelle position and epithelial architecture associated with loss of CrebA. *Biol Open*, *4*(3), 317-330. https://doi.org/10.1242/bio.201411205

Fox, R. M., Vaishnavi, A., Maruyama, R., & Andrew, D. J. (2013). Organ-specific gene expression: the bHLH protein Sage provides tissue specificity to Drosophila FoxA. *Development*, *140*(10), 2160-2171. https://doi.org/10.1242/dev.092924

Ghosh, N., & Treisman, J. E. (2024). Apical cell expansion maintained by Dusky-like establishes a scaffold for corneal lens morphogenesis. *Sci Adv*, *10*(34), eado4167. https://doi.org/10.1126/sciadv.ado4167

Gill, H. K., Cohen, J. D., Ayala-Figueroa, J., Forman-Rubinsky, R., Poggioli, C., Bickard, K., Parry, J. M., Pu, P., Hall, D. H., & Sundaram, M. V. (2016). Integrity of Narrow Epithelial Tubes in the C. elegans Excretory System Requires a Transient Luminal Matrix. *PLoS Genet*, *12*(8), e1006205. https://doi.org/10.1371/journal.pgen.1006205

Groza, T., Gomez, F. L., Mashhadi, H. H., Munoz-Fuentes, V., Gunes, O., Wilson, R., Cacheiro, P., Frost, A., Keskivali-Bond, P., Vardal, B., McCoy, A., Cheng, T. K., Santos, L., Wells, S., Smedley, D., Mallon, A. M., & Parkinson, H. (2023). The International Mouse Phenotyping Consortium: comprehensive knockout phenotyping underpinning the study

of human disease. *Nucleic Acids Res*, *51*(D1), D1038-D1045. https://doi.org/10.1093/nar/gkac972
Gunal, S., Hardman, R., Kopriva, S., & Mueller, J. W. (2019). Sulfation pathways from red to green. *J Biol Chem*, *294*(33), 12293-12312. https://doi.org/10.1074/jbc.REV119.007422
Gyoergy, A., Roblek, M., Ratheesh, A., Valoskova, K., Belyaeva, V., Wachner, S., Matsubayashi, Y., Sanchez-Sanchez, B. J., Stramer, B., & Siekhaus, D. E. (2018). Tools Allowing Independent Visualization and Genetic Manipulation of Drosophila melanogaster Macrophages and Surrounding Tissues. *G3 (Bethesda)*, *8*(3), 845-857. https://doi.org/10.1534/g3.117.300452
Herman, T., & Horvitz, H. R. (1999). Three proteins involved in Caenorhabditis elegans vulval invagination are similar to components of a glycosylation pathway. *Proc Natl Acad Sci U S A*, *96*(3), 974-979. https://doi.org/10.1073/pnas.96.3.974
Hwang, H. Y., Olson, S. K., Brown, J. R., Esko, J. D., & Horvitz, H. R. (2003). The Caenorhabditis elegans genes sqv-2 and sqv-6, which are required for vulval morphogenesis, encode glycosaminoglycan galactosyltransferase II and xylosyltransferase. *J Biol Chem*, *278*(14), 11735-11738. https://doi.org/10.1074/jbc.C200518200
Ismat, A., Cheshire, A. M., & Andrew, D. J. (2013). The secreted AdamTS-A metalloprotease is required for collective cell migration. *Development*, *140*(9), 1981-1993. https://doi.org/10.1242/dev.087908
Jazwinska, A., & Affolter, M. (2004). A family of genes encoding zona pellucida (ZP) domain proteins is expressed in various epithelial tissues during Drosophila embryogenesis. *Gene Expr Patterns*, *4*(4), 413-421. https://doi.org/10.1016/j.modgep.2004.01.003
Jazwinska, A., Ribeiro, C., & Affolter, M. (2003). Epithelial tube morphogenesis during Drosophila tracheal development requires Piopio, a luminal ZP protein. *Nat Cell Biol*, *5*(10), 895-901. https://doi.org/10.1038/ncb1049
Jovine, L., Darie, C. C., Litscher, E. S., & Wassarman, P. M. (2005). Zona pellucida domain proteins. *Annu Rev Biochem*, *74*, 83-114. https://doi.org/10.1146/annurev.biochem.74.082803.133039
Jovine, L., Qi, H., Williams, Z., Litscher, E., & Wassarman, P. M. (2002). The ZP domain is a conserved module for polymerization of extracellular proteins. *Nat Cell Biol*, *4*(6), 457-461. https://doi.org/10.1038/ncb802
Jullien, D., Crozatier, M., & Kas, E. (1997). cDNA sequence and expression pattern of the Drosophila melanogaster PAPS synthetase gene: a new salivary gland marker. *Mech Dev*, *68*(1-2), 179-186. https://doi.org/10.1016/s0925-4773(97)00136-6
Kamiyama, S., Suda, T., Ueda, R., Suzuki, M., Okubo, R., Kikuchi, N., Chiba, Y., Goto, S., Toyoda, H., Saigo, K., Watanabe, M., Narimatsu, H., Jigami, Y., & Nishihara, S. (2003). Molecular cloning and identification of 3'-phosphoadenosine 5'-phosphosulfate transporter. *J Biol Chem*, *278*(28), 25958-25963. https://doi.org/10.1074/jbc.M302439200
Karlsson, M., Zhang, C., Mear, L., Zhong, W., Digre, A., Katona, B., Sjostedt, E., Butler, L., Odeberg, J., Dusart, P., Edfors, F., Oksvold, P., von Feilitzen, K., Zwahlen, M., Arif, M., Altay, O., Li, X., Ozcan, M., Mardinoglu, A.,…Lindskog, C. (2021). A single-cell type transcriptomics map of human tissues. *Sci Adv*, *7*(31). https://doi.org/10.1126/sciadv.abh2169

Kondylis, V., & Rabouille, C. (2009). The Golgi apparatus: lessons from Drosophila. *FEBS Lett*, *583*(23), 3827-3838. https://doi.org/10.1016/j.febslet.2009.09.048

Kurima, K., Warman, M. L., Krishnan, S., Domowicz, M., Krueger, R. C., Jr., Deyrup, A., & Schwartz, N. B. (1998). A member of a family of sulfate-activating enzymes causes murine brachymorphism. *Proc Natl Acad Sci U S A*, *95*(15), 8681-8685. https://doi.org/10.1073/pnas.95.15.8681

Le, T. P., & Chung, S. (2021). Regulation of apical constriction via microtubule- and Rab11-dependent apical transport during tissue invagination. *Mol Biol Cell*, *32*(10), 1033-1047. https://doi.org/10.1091/mbc.E21-01-0021

Li Zheng, S., Adams, J. G., & Chisholm, A. D. (2020). Form and function of the apical extracellular matrix: new insights from Caenorhabditis elegans, Drosophila melanogaster, and the vertebrate inner ear. *Fac Rev*, *9*, 27. https://doi.org/10.12703/r/9-27

Litscher, E. S., & Wassarman, P. M. (2020). Zona pellucida genes and proteins and human fertility. *Trends Dev Biol*, *13*, 21-33. https://www.ncbi.nlm.nih.gov/pubmed/33335361

Liu, X., Zhang, J., & Zhu, K. Y. (2019). Chitin in Arthropods: Biosynthesis, Modification, and Metabolism. *Adv Exp Med Biol*, *1142*, 169-207. https://doi.org/10.1007/978-981-13-7318-3_9

Luders, F., Segawa, H., Stein, D., Selva, E. M., Perrimon, N., Turco, S. J., & Hacker, U. (2003). Slalom encodes an adenosine 3'-phosphate 5'-phosphosulfate transporter essential for development in Drosophila. *EMBO J*, *22*(14), 3635-3644. https://doi.org/10.1093/emboj/cdg345

Luschnig, S., Batz, T., Armbruster, K., & Krasnow, M. A. (2006). serpentine and vermiform encode matrix proteins with chitin binding and deacetylation domains that limit tracheal tube length in Drosophila. *Curr Biol*, *16*(2), 186-194. https://doi.org/10.1016/j.cub.2005.11.072

Lye, C. M., Naylor, H. W., & Sanson, B. (2014). Subcellular localisations of the CPTI collection of YFP-tagged proteins in Drosophila embryos. *Development*, *141*(20), 4006-4017. https://doi.org/10.1242/dev.111310

Matthew, J., Vishwakarma, V., Le, T. P., Agsunod, R. A., & Chung, S. (2024). Coordination of cell cycle and morphogenesis during organ formation. *Elife*, *13*. https://doi.org/10.7554/eLife.95830

McAllister, K. A., Grogg, K. M., Johnson, D. W., Gallione, C. J., Baldwin, M. A., Jackson, C. E., Helmbold, E. A., Markel, D. S., McKinnon, W. C., Murrell, J., & et al. (1994). Endoglin, a TGF-beta binding protein of endothelial cells, is the gene for hereditary haemorrhagic telangiectasia type 1. *Nat Genet*, *8*(4), 345-351. https://doi.org/10.1038/ng1294-345

Moussian, B., Tang, E., Tonning, A., Helms, S., Schwarz, H., Nusslein-Volhard, C., & Uv, A. E. (2006). Drosophila Knickkopf and Retroactive are needed for epithelial tube growth and cuticle differentiation through their specific requirement for chitin filament organization. *Development*, *133*(1), 163-171. https://doi.org/10.1242/dev.02177

Myat, M. M., & Andrew, D. J. (2000a). Fork head prevents apoptosis and promotes cell shape change during formation of the Drosophila salivary glands. *Development*, *127*(19), 4217-4226. https://doi.org/10.1242/dev.127.19.4217

Myat, M. M., & Andrew, D. J. (2000b). Organ shape in the Drosophila salivary gland is controlled by regulated, sequential internalization of the primordia. *Development*, *127*(4), 679-691. https://doi.org/10.1242/dev.127.4.679

Myat, M. M., & Andrew, D. J. (2002). Epithelial tube morphology is determined by the polarized growth and delivery of apical membrane. *Cell*, *111*(6), 879-891. https://doi.org/10.1016/s0092-8674(02)01140-6

Negishi, M., Pedersen, L. G., Petrotchenko, E., Shevtsov, S., Gorokhov, A., Kakuta, Y., & Pedersen, L. C. (2001). Structure and function of sulfotransferases. *Arch Biochem Biophys*, *390*(2), 149-157. https://doi.org/10.1006/abbi.2001.2368

Plaza, S., Chanut-Delalande, H., Fernandes, I., Wassarman, P. M., & Payre, F. (2010). From A to Z: apical structures and zona pellucida-domain proteins. *Trends Cell Biol*, *20*(9), 524-532. https://doi.org/10.1016/j.tcb.2010.06.002

Renner, M., Bergmann, G., Krebs, I., End, C., Lyer, S., Hilberg, F., Helmke, B., Gassler, N., Autschbach, F., Bikker, F., Strobel-Freidekind, O., Gronert-Sum, S., Benner, A., Blaich, S., Wittig, R., Hudler, M., Ligtenberg, A. J., Madsen, J., Holmskov, U.,…Mollenhauer, J. (2007). DMBT1 confers mucosal protection in vivo and a deletion variant is associated with Crohn's disease. *Gastroenterology*, *133*(5), 1499-1509. https://doi.org/10.1053/j.gastro.2007.08.007

Rutherford, S. A., Goldberg, M. W., & Allen, T. D. (1997). Three-dimensional visualization of the route of protein import: the role of nuclear pore complex substructures. *Exp Cell Res*, *232*(1), 146-160. https://doi.org/10.1006/excr.1997.3487

Sarkissian, T., Timmons, A., Arya, R., Abdelwahid, E., & White, K. (2014). Detecting apoptosis in Drosophila tissues and cells. *Methods*, *68*(1), 89-96. https://doi.org/10.1016/j.ymeth.2014.02.033

Smith, S. J., Davidson, L. A., & Rebeiz, M. (2020). Evolutionary expansion of apical extracellular matrix is required for the elongation of cells in a novel structure. *Elife*, *9*. https://doi.org/10.7554/eLife.55965

Suiko, M., Fernando, P. H., Sakakibara, Y., Nakajima, H., Liu, M. C., Abe, S., & Nakatsu, S. (1992). Post-translational modification of protein by tyrosine sulfation: active sulfate PAPS is the essential substrate for this modification. *Nucleic Acids Symp Ser*(27), 183-184. https://www.ncbi.nlm.nih.gov/pubmed/1289811

Syed, Z. A., Bouge, A. L., Byri, S., Chavoshi, T. M., Tang, E., Bouhin, H., van Dijk-Hard, I. F., & Uv, A. (2012). A luminal glycoprotein drives dose-dependent diameter expansion of the Drosophila melanogaster hindgut tube. *PLoS Genet*, *8*(8), e1002850. https://doi.org/10.1371/journal.pgen.1002850

Tang, W. J., Fernandez, J., Sohn, J. J., & Amemiya, C. T. (2015). Chitin is endogenously produced in vertebrates. *Curr Biol*, *25*(7), 897-900. https://doi.org/10.1016/j.cub.2015.01.058

Tomancak, P., Beaton, A., Weiszmann, R., Kwan, E., Shu, S., Lewis, S. E., Richards, S., Ashburner, M., Hartenstein, V., Celniker, S. E., & Rubin, G. M. (2002). Systematic determination of patterns of gene expression during Drosophila embryogenesis. *Genome Biol*, *3*(12), RESEARCH0088. https://doi.org/10.1186/gb-2002-3-12-research0088

Tonning, A., Helms, S., Schwarz, H., Uv, A. E., & Moussian, B. (2006). Hormonal regulation of mummy is needed for apical extracellular matrix formation and epithelial morphogenesis in Drosophila. *Development*, *133*(2), 331-341. https://doi.org/10.1242/dev.02206

Tonning, A., Hemphala, J., Tang, E., Nannmark, U., Samakovlis, C., & Uv, A. (2005). A transient luminal chitinous matrix is required to model epithelial tube diameter in the Drosophila trachea. *Dev Cell*, *9*(3), 423-430. https://doi.org/10.1016/j.devcel.2005.07.012

Uhlen, M., Bjorling, E., Agaton, C., Szigyarto, C. A., Amini, B., Andersen, E., Andersson, A. C., Angelidou, P., Asplund, A., Asplund, C., Berglund, L., Bergstrom, K., Brumer, H., Cerjan, D., Ekstrom, M., Elobeid, A., Eriksson, C., Fagerberg, L., Falk, R.,…Ponten, F. (2005). A human protein atlas for normal and cancer tissues based on antibody proteomics. *Mol Cell Proteomics*, *4*(12), 1920-1932. https://doi.org/10.1074/mcp.M500279-MCP200

van den Boom, J., Heider, D., Martin, S. R., Pastore, A., & Mueller, J. W. (2012). 3'-Phosphoadenosine 5'-phosphosulfate (PAPS) synthases, naturally fragile enzymes specifically stabilized by nucleotide binding. *J Biol Chem*, *287*(21), 17645-17655. https://doi.org/10.1074/jbc.M111.325498

Venkatachalam, K. V., Akita, H., & Strott, C. A. (1998). Molecular cloning, expression, and characterization of human bifunctional 3'-phosphoadenosine 5'-phosphosulfate synthase and its functional domains. *J Biol Chem*, *273*(30), 19311-19320. https://doi.org/10.1074/jbc.273.30.19311

Wang, S., Jayaram, S. A., Hemphala, J., Senti, K. A., Tsarouhas, V., Jin, H., & Samakovlis, C. (2006). Septate-junction-dependent luminal deposition of chitin deacetylases restricts tube elongation in the Drosophila trachea. *Curr Biol*, *16*(2), 180-185. https://doi.org/10.1016/j.cub.2005.11.074

Weiszmann, R., Hammonds, A. S., & Celniker, S. E. (2009). Determination of gene expression patterns using high-throughput RNA in situ hybridization to whole-mount Drosophila embryos. *Nat Protoc*, *4*(5), 605-618. https://doi.org/10.1038/nprot.2009.55

Wilkin, M. B., Becker, M. N., Mulvey, D., Phan, I., Chao, A., Cooper, K., Chung, H. J., Campbell, I. D., Baron, M., & MacIntyre, R. (2000). Drosophila dumpy is a gigantic extracellular protein required to maintain tension at epidermal-cuticle attachment sites. *Curr Biol*, *10*(10), 559-567. https://doi.org/10.1016/s0960-9822(00)00482-6

Wong, S. H., Hamel, L., Chevalier, S., & Philip, A. (2000). Endoglin expression on human microvascular endothelial cells association with betaglycan and formation of higher order complexes with TGF-beta signalling receptors. *Eur J Biochem*, *267*(17), 5550-5560. https://doi.org/10.1046/j.1432-1327.2000.01621.x

Xia, B., Royall, J. A., Damera, G., Sachdev, G. P., & Cummings, R. D. (2005). Altered O-glycosylation and sulfation of airway mucins associated with cystic fibrosis. *Glycobiology*, *15*(8), 747-775. https://doi.org/10.1093/glycob/cwi061

Yan, B., Zhang, Z. Z., Huang, L. Y., Shen, H. L., & Han, Z. G. (2012). OIT3 deficiency impairs uric acid reabsorption in renal tubule. *FEBS Lett*, *586*(6), 760-765. https://doi.org/10.1016/j.febslet.2012.01.038

Yanagisawa, K., Sakakibara, Y., Suiko, M., Takami, Y., Nakayama, T., Nakajima, H., Takayanagi, K., Natori, Y., & Liu, M. C. (1998). cDNA cloning, expression, and characterization of the human bifunctional ATP sulfurylase/adenosine 5'-phosphosulfate kinase enzyme. *Biosci Biotechnol Biochem*, *62*(5), 1037-1040. https://doi.org/10.1271/bbb.62.1037

Ye, B., Zhang, Y., Song, W., Younger, S. H., Jan, L. Y., & Jan, Y. N. (2007). Growing dendrites and axons differ in their reliance on the secretory pathway. *Cell*, *130*(4), 717-729. https://doi.org/10.1016/j.cell.2007.06.032

Zhang, Y., Foster, J. M., Nelson, L. S., Ma, D., & Carlow, C. K. (2005). The chitin synthase genes chs-1 and chs-2 are essential for C. elegans development and responsible for chitin

deposition in the eggshell and pharynx, respectively. *Dev Biol*, *285*(2), 330-339. https://doi.org/10.1016/j.ydbio.2005.06.037

Zhu, X., Sen, J., Stevens, L., Goltz, J. S., & Stein, D. (2005). Drosophila pipe protein activity in the ovary and the embryonic salivary gland does not require heparan sulfate glycosaminoglycans. *Development*, *132*(17), 3813-3822. https://doi.org/10.1242/dev.01962